Dissertation

MECHANISMS BEHIND OMEGA-3 FATTY ACIDS ' ANTI-PROLIFERATIVE EFFECT ON HUMAN PULMONARY ARTERY SMOOTH MUSCLE CELLS

submitted by

D.I.
Slaven CRNKOVIC

for the academic degree of

Doctor of Philosophy
(Ph.D.)

at the

Medical University of Graz
Institute for Molecular Biology and Biochemistry/
University Clinic of Anesthesiology and Intensive Care Medicine

under Supervision of

Prof. Dr. Sasa FRANK

and

Prof. Dr. Andrea OLSCHEWSKI

Declaration

I hereby declare that this thesis is my own original work and that I have fully acknowledged by name all of those individuals and organizations that have contributed to the research for this thesis. Due acknowledgement has been made in the text to all other material used. Throughout this thesis and in all related publications I followed the guidelines of "Good Scientific Practice".

Graz, [date & signature]

Acknowledgements

I would like to kindly thank my mentors Sasa Frank and Andrea Olschewski for giving me the opportunity to develop both as a person and as a scientist; Monika Riederer for her guidance and help during the course of my PhD study; Snjezana Cuzic for explaining me the lung morphology; Nagaraj Chandran for helpful discussions and practical advices; Lada Brkic for helpful encouragements and patience and Margarete Lechleitner for practical help in critical moments.

TABLE OF CONTENTS

ABBREVIATIONS

AA – arachidonic acid

ATP – adenosine triphosphate

DAPI – 4',6-diamidino-2-phenylindole

DHA – docosahexaenoic acid

$\Delta\Psi_m$ – mitochondrial membrane potential

eIF-2α – eukaryotic initiation factor 2 alpha

EPA – eicosapentaenoic acid

ER – endoplasmic-reticulum

ERAD – endoplasmic-reticulum-associated protein degradation

FCS – fetal calf serum

H_2DCFDA – 2', 7'-dichlorohihydrofluorescein diacetate (

HO-1 – heme oxygenase 1

hPASMC – human pulmonary artery smooth muscle cells

IRE1 – inositol-requiring kinase 1

LDL –- low density lipoprotein

LINO – alpha linolenic acid

mRNA – messenger ribonucleic acid

n-3 PUFA – n-3 polyunsaturated fatty acids

PAH – pulmonary arterial hypertension

PBS – phosphate buffered saline

PDGF – platelet-derived growth factor

PDI – disulphide isomerase

PERK – PRKR-like ER kinase

PH – pulmonary hypertension

PI – propidium iodide

PPAR – peroxisome proliferator receptor

PUFA – polyunsaturated fatty acids

qRT-PCR – quantitative reverse-transcription polymerase chain reaction

ROS – reactive oxygen species

SEM – standard error of the mean

UPR – unfolded protein response

VEGF – vascular endothelial growth factor

veh – vehicle

VLDL – very low density lipoprotein

XBP-1 – X-box binding protein 1

ZUSAMENFASSUNG

Ein charakteristisches Merkmal für einen pathologischen Gefäßumbau ist die Proliferation (Zellwucherung) der glatten Gefäßmuskelzellen, welche bei einigen kardiovaskulären Erkrankungen eine bedeutende therapeutische Herausforderung darstellt. Docosahexaensäure (DHA), welche zu den n-3 mehrfach ungesättigten Fettsäuren (n-3 PUFA) gehört, hemmt die Proliferation zahlreicher Zelltypen, was auf unterschiedliche Wirkmechanismen hindeutet. In der vorliegenden Studie haben wir jene molekularen Ereignisse untersucht, die der hemmenden Wirkung von DHA auf die Proliferation von primären menschlichen glatten Muskelzellen (hPASMC), isoliert aus der kleinen Lungenarterien, zu Grunde liegen.

DHA hemmte konzentrationsabhängig die hPASMC-Proliferation, induzierte den G1 Zellzyklus-Stopp und verringerte die Zyklin D1 Proteinexpression. DHA aktivierte außerdem die Antwort entfalteter Proteine (UPR), was durch eine erhöhte mRNA-Expression von HSPA5, durch eine verringerte Phosphorylierung des eukaryotischen Initiationsfaktors 2 alpha (eIF-2α) und durch das Spleißen des X-Box Binding Proteins 1 (XBP-1) bewiesen wurde. DHA veränderte die zelluläre Fettzusammensetzung und führte weiters zur verstärkten Produktion von reaktiven Sauerstoffspezies (ROS).

DHA induzierte ROS waren sowohl von der intrazellulären Kalziumabgabe als auch vom Eintritt des extrazellulären Kalziums in die Zellen abhängig. Zelluläre ROS und mitochondriale ROS wurden durch RU360, einem spezifischen Inhibitor der mitochondrialen Kalziumaufnahme, verringert. Die DHA induzierte mitochondriale Funktionsstörung wurde durch ein verringertes mitochondriales Membranpotential und durch einen verringerten zellulären ATP-Gehalt bewiesen. DHA löste Apoptose aus, wie wir durch die verringerte Anzahl von gespaltener Caspase 3 und TUNEL positiven Zellen herausgefunden haben. Der freie Radikalfänger Tempol hingegen wirkt den DHA induzierten ROS, Zellzyklus-Stopp, UPR-Induktion und Apoptose entgegen.

Wir schlussfolgern daher, dass Kalzium-abhängiger oxidativer Stress das zentrale und anfängliche Ereignis ist, das für UPR-Induktion, Zellzyklus-Stopp und Apoptose in DHA behandelten hPASM-Zellen verantwortlich ist.

SUMMARY

Proliferation of vascular smooth muscle cells is a characteristic of pathological vascular remodeling and represents a significant therapeutic challenge in several cardiovascular diseases. Docosahexaenoic acid (DHA), a member of n-3 polyunsaturated fatty acids (n-3 PUFA), was shown to inhibit proliferation of numerous cell types implicating several different mechanisms. In the present study we examined molecular events underlying the inhibitory effect of DHA on proliferation of primary human smooth muscle cells isolated from small pulmonary arteries (hPASMC).

DHA concentration-dependently inhibited hPASMC proliferation, induced G1 cell cycle arrest and decreased cyclin D1 protein expression. DHA activated the unfolded protein response (UPR), evidenced by increased mRNA expression of HSPA5, increased phosphorylation of eukaryotic initiation factor 2 alpha (eIF-2α) and splicing of X-box binding protein 1 (XBP-1). DHA altered the cellular lipid composition and led to increased reactive oxygen species (ROS) production.

DHA-induced ROS was dependent on both, intracellular Ca^{2+} release and entry of extracellular Ca^{2+}. Overall, cellular ROS and mitochondrial ROS were decreased by RU360, a specific inhibitor of mitochondrial Ca^{2+} uptake. DHA –induced mitochondrial dysfunction was evidenced by decreased mitochondrial membrane potential ($\Delta\Psi_m$) and decreased cellular ATP content. DHA triggered apoptosis as found by increased number of cleaved caspase-3 and TUNEL positive cells. Free radical scavenger, Tempol, counteracted DHA-induced ROS, cell cycle arrest, induction of UPR and apoptosis.

We concluded that Ca^{2+}-dependent oxidative stress is the central and initial event responsible for the induction of UPR, cell cycle arrest and apoptosis in DHA-treated hPASMC.

1. INTRODUCTION

Pathologic vascular remodeling is a hallmark in several cardiovascular diseases, such as pulmonary hypertension and stent restenosis (1,2), and represents a significant therapeutic challenge. Aberrant proliferation of vascular smooth muscle cells is a characteristic feature of pathological vascular remodeling which results in narrowing and obliteration of blood vessels. Together with intravessel thrombosis and vasoconstriction, it causes increased vascular resistance. This affects the heart and leads to ventricular hypertrophy which progresses with time to decompensated heart failure and death. These pathological processes are particularly evident and pronounced in pulmonary hypertension.

1.1. PULMONARY HYPERTENSION

Pulmonary hypertension is a syndrome in which increased pulmonary vascular resistance, either due to narrowing of pulmonary artery lumen or obstruction of outflow through the pulmonary venous system, leads to increased workload on the right ventricle (3). It is a progressive and incurable disease of the pulmonary vasculature and is defined as increased mean pulmonary artery pressure above 25 mmHg (4). With time, the right ventricle can no longer cope with the increasing functional demand to pump the blood against increasing pulmonary vascular resistance. Therefore, in the final stage of the disease, pulmonary hypertension leads to right ventricular failure and a 15% annual mortality rate (3).

Pulmonary hypertension is divided in 5 groups according to the latest World Health Organization (WHO) clinical classification (Table 1).

Group I Pulmonary arterial hypertension

- Idiopathic
- Heritable:
  - BMPR2 mutations
  - ALK1, endoglin mutations
  - unknown mutations
- Drugs or toxins induced
- Associated with:
  - connective tissue disease
  - portal hypertension
  - HIV infection
  - congenital heart disease
  - schistosomiasis
  - chronic hemolytic anemia
- Persistent pulmonary hypertension of the newborn
- Pulmonary veno-occlusive disease (PVOD) and/or pulmonary capillary hemangiomatosis (PCH)

Group II Pulmonary hypertension due to left heart disease

- Systolic dysfunction
- Diastolic dysfunction
- Valvular disease

Group III Pulmonary hypertension due to lung diseases and/or hypoxemia

- Chronic obstructive lung disease
- Interstitial lung disease
- Other pulmonary diseases with mixed restrictive/obstructive pattern
- Sleep-disordered breathing
- Alveolar hypoventilation disorders
- Chronic exposure to high altitude
- Developmental abnormalities

Group IV Pulmonary hypertension due to chronic thrombotic disease, embolic disease, or both

- Thromboembolic obstruction of proximal pulmonary arteries
- Thromboembolic obstruction of distal pulmonary arteries
- Pulmonary embolism (tumor, parasites, foreign material)

Group V Pulmonary hypertension with unclear or multifactorial mechanisms

- Hematologic disorders
  - myeloproliferative disorders
  - splenectomy
- Systemic disorders
  - sarcoidosis
  - pulmonary Langerhans' cell histiocytosis
  - lymphangiomatosis
  - neurofibromatosis,
  - vasculitis
- Metabolic disorders
  - glycogen storage disease
  - Gaucher disease
  - thyroid disorders
- Others
  - tumoral obstruction
  - fibrosing mediastinitis
  - chronic renal
  - failure on hemodialysis

Table 1. Dana Point clinical classification of pulmonary hypertension.

Numerous morphological, cellular and molecular abnormalities were found in the pulmonary vasculature of affected patients (5). Key pathological features of pulmonary hypertension are pulmonary vasoconstriction and pulmonary vascular remodeling. Even though the exact processes that initiate these pathological changes are still unknown, research indicates that pulmonary hypertension has a multi-factorial pathobiology that involves various biochemical pathways and cell types (4).

Functional changes include all three major cell types present in the pulmonary vessels: endothelial cells, smooth muscle cells and adventitial fibroblasts. The increase of pulmonary vascular resistance is related to different mechanisms including vasoconstriction, obstructive remodeling of the pulmonary vessel wall, inflammation and thrombosis (4).

One of the first described changes was pulmonary endothelial dysfunction. Generally, it is characterized by an altered balance in the production of vasoconstrictive and vasodilating factors. Pulmonary hypertension patients have increased levels of vasoconstrictive factors such as thromboxane A_2 and endothelin and at the same time decreased levels of vasodilating factors such as nitric oxide and prostacyclin (6). On one hand, these abnormalities lead to pulmonary vasoconstriction and on the other hand, they promote pathological vascular remodeling (4). Targeting endothelial dysfunction is the only therapeutic option for the vast majority of pulmonary hypertension patients (7). Approved classes of medications include endothelin receptor antagonsists, stabile prostacyclin analogues and phosphodiesterase type V inhibitors. Although pulmonary vasoconstriction is believed to be an early component of the pulmonary hypertensive process (8), available therapy options only ameliorate and partially slow down the progression of the disease but do not provide a definitive cure.

In addition to endothelial dysfunction, excessive vasoconstriction has been related to functional changes in smooth muscle cells. These include a proliferative smooth

muscle cell phenotype, changes in the activity of potassium channels (9) and an altered expression of the serotonin transporters (5).

Similarly, adventitial fibroblasts display an increased proliferative capacity (10) and increased production of extracellular matrix including collagen, elastin, fibronectin, and tenascin (11) contributing further to pathologic pulmonary vascular remodeling.

Histopathological features of pulmonary vascular remodeling that is present in pulmonary vessels from pulmonary hypertension patients include medial hypertrophy, intimal thickening, adventitial thickening and complex lesions (4). This process involves all layers of the vessel wall and is characterized by proliferative and obstructive changes that involve several cell types including endothelial, smooth muscle cells and fibroblasts (12).

Intimal thickening can be defined as concentric laminar, eccentric or concentric non-laminar. Ultrastructurally and immuno-histochemically the intimal cells show features and markers of fibroblasts, myofibroblasts and smooth muscle cells origin (4). Of importance, recent characterization of morphological features revealed that the primary difference between the PAH and control groups resides largely in the intima thickening (7).

Medial hypertrophy is an increase in the cross sectional area of the media of pre and intra-acinar pulmonary arteries. It is due to both hypertrophy and hyperplasia of smooth muscle fibers as well as increase in connective tissue matrix and elastic fibers in the media of muscular arteries (4). Although previously thought to be a major determinant and cause of increased pulmonary vascular resistance, due to its contribution to the narrowing of the vessel lumen, medial hypertrophy measured in pulmonary hypertension patients was similar to that measured in normal control subjects (7).

Even though adventitial thickening occurs in most cases of PAH due to methodological difficulties its assessment and quantification is lacking a systematic review (4).

Unique feature of vascular remodeling occurring in pulmonary arterial hypertension are omplex or plexiform lesions (7). The plexiform lesion is a focal proliferation of endothelial channels lined by myofibroblasts, smooth muscle cells and connective tissue matrix (4). These lesions are at an arterial branching point or at the origin of a supernumerary artery, distally to marked obliterative intimal thickening of the parent artery (4).

In addition to resident vascular cells, circulating cells such as inflammatory cells and platelets may play a significant role in PAH (4). In fact, inflammatory cells are ubiquitous in PAH pathological changes and pro-inflammatory cytokines are elevated in the plasma of PAH patients (13). Furthermore, inflammatory cell infiltrates are observed both intra and perivasculary in the lungs of PAH patients (7).

Besides vasoconstrictive and proinflammatory changes, prothrombotic abnormalities have also been detected in PAH patients (14). Furthermore, thrombi are present in both microcirculation and elastic pulmonary arteries (12).

An additional factor that is stored and released by platelets is platelet-derived growth factor (PDGF). PDGF is a potent mitogen for vascular smooth muscle cells. Reports have shown that the expression of the PDGF receptor is significantly increased in lung tissue from pulmonary arterial hypertension patients compared with healthy donor lung tissue (15). Furthermore, PDGF receptor antagonists reversed advanced pulmonary vascular disease in two animal models of pulmonary hypertension (15).

Finally, genetic changes, such as mutations in the BMPR2 receptor, also play a role in the development and initiation of pulmonary hypertension. It is assumed

that the interaction between genetic predisposition and risk factors that may induce changes in different cell types (smooth muscle cells, endothelial cells, inflammatory cells, platelets) and in the extracellular matrix of pulmonary microcirculation govern the development of pulmonary hypertension (4).

In order to study the pathomechanism of pulmonary hypertension, several animal models have been developed and used over time. However, no animal model completely recapitulates human PH (3). Most widely used are rodent models of experimental PH. Rat models of group 1 PH include: monocrotaline (± pneumonectomy), chronic hypoxia + SU-5416 (a VEGF receptor inhibitor) and the fawn-hooded rat (FHR) (16). Mouse models of group 1 PH include: transgenic mice overexpressing the serotonin transporter or dominant-negative mutants of bone morphogenetic protein receptor-2 (16). Group 1 PH is also created by infecting S100A4/Mts1 mice with γ-herpesvirus (16). Group 3 PH is modeled by exposure of rats or mice to chronic hypoxia (16).

Despite decades of intense research to discover the pathomechanisms and develop potential novel drug therapies, lung transplantation still remains the only curative option for these patients. Therefore, novel therapies targeting the vascular remodeling process are urgently needed.

1.2. OMEGA-3 POLYUNSATURATED FATTY ACIDS

Omega-3 fatty acids (ω−3 fatty acids or n−3 fatty acids) represent a group of polyunsaturated fatty acids (PUFAs). They are naturally occurring molecules with all double bonds in cis conformation and with the first double bond positioned at the third carbon form the methyl end (omega carbon) of the molecule (Table 2). They differ in the length of the acyl chain and the number of double bonds. Physiologically most relevant omega-3 fatty acids are alpha-linolenic (ALA), eicosapentaenoic (EPA) and docosahexaenoic acid (DHA) (Table 2).

From a nutritional point of view, ALA is considered as “essential” fatty acid, since it is not synthesized in the human body and is mostly obtained from the diet (17).

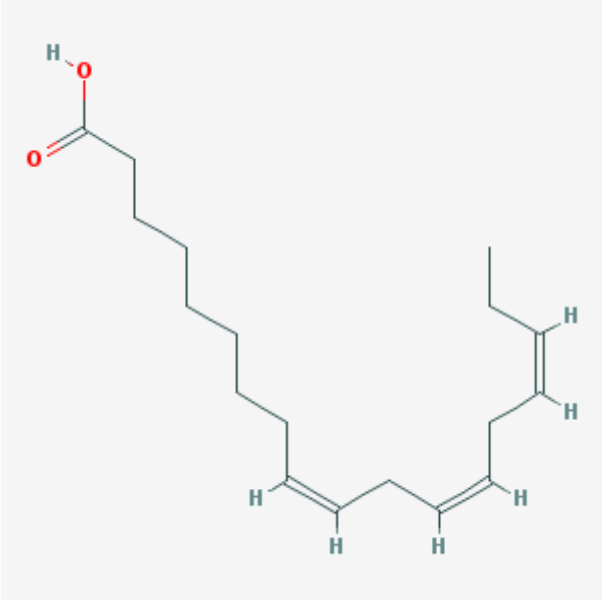

α-Linolenic acid (ALA)

18:3 (n−3)

all-cis-9,12,15-octadecatrienoic acid

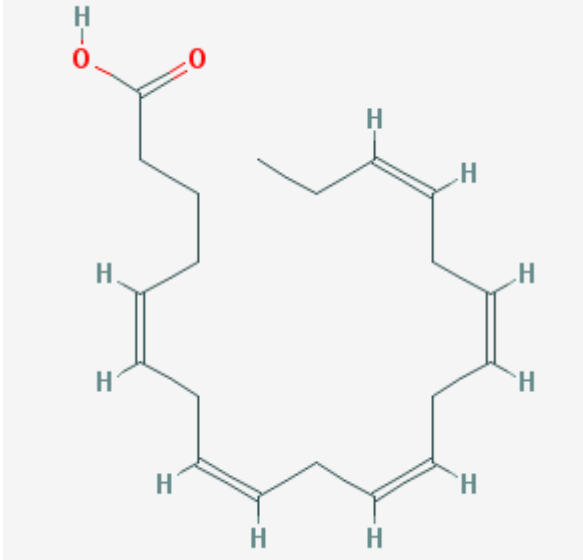

Eicosapentaenoic acid (EPA)

20:5 (n−3)

all-cis-5,8,11,14,17-eicosapentaenoic acid

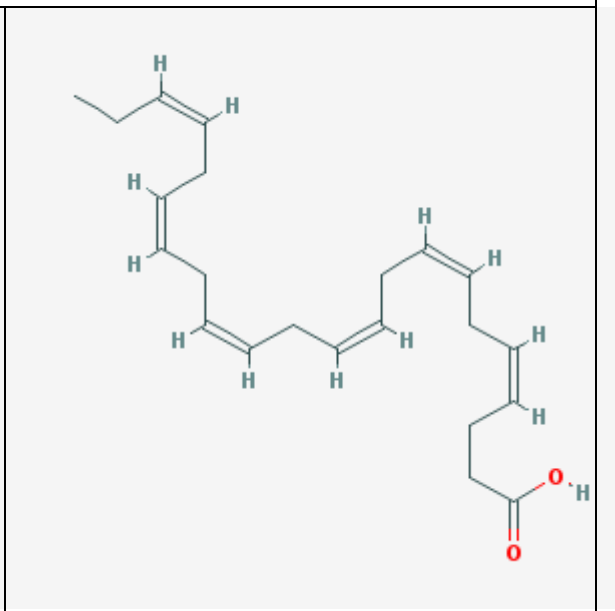

Docosahexaenoic acid (DHA)

22:6 (n−3)

all-cis-4,7,10,13,16,19-docosahexaenoic acid

Table 2. Structures of physiologically relevant omega-3 fatty acids. Source: NCBI PubChem Compound database.

Non-esterified omega-3 fatty acids present in the diet are rapidly and efficiently absorbed, enter cells via fatty acid transporters where they are rapidly converted to fatty acids acyl-CoA thioesters, before undergoing metabolic fates (17). They either contribute to ATP production by the classical beta-oxidation pathway following acyl-chain shortening in peroxysomes (17), are converted in long chain omega-3 PUFAs by the activities of consecutive desaturation and elongation reactions (17) or they are incorporated in cellular phospholipids and triglycerides.

Since biosynthesis of fatty acids and phospholipids occurs in the endoplasmic reticulum, the intermediates of the PUFA metabolism can either be incorporated into phospholipids, or become the substrate for a further elongation/ desaturation reaction (17). In the membranes, PUFAs contribute to their fluidity that is an important determinant for the correct hormone-receptor binding, which is a function of the fluidity of cell membranes (17).

Omega-3 fatty acids can act in intracellular signaling as second messengers when incorporated in the cell membrane (17). Following the activation of phospholipase A2, EPA and DHA are cleaved and released from sn-2 position of phospholipids (17). Depending on the activities of downstream processing enzymes, such as cyclooxygenases (COX-1 and COX-2), lipoxygenases (5-, 12-, or 15-LOX), or cytochrome P450 monoxygenases, omega-3 PUFAs can act as substrates for the biosynthesis of series 3 prostanoids, such as PGI_3, PGE_3 etc. (17).

Furthermore, omega-3 fatty acids can rapidly modulate gene expression by acting as ligands for several transcription factors such as peroxisome proliferator receptors (PPARs), liver X receptors (LXRs) and sterol regulatory element-binding protein 1c (SREBP-1c) (17).

Esters of EPA and DHA are used clinically to treat hypertriglyceridemia. However, several epidemiological and experimental studies suggested that omega-3 PUFAs could exert additional favorable cardiovascular effects (18). A large-scale, randomised, placebo-controlled trial showed that n-3 PUFA could improve morbidity and mortality of patients with symptomatic heart failure of any cause and with any level of left ventricular ejection fraction (LVEF) (19).

There is indirect evidence that the beneficial effects of omega-3 fatty acids may be due to their ability to inhibit smooth muscle cell proliferation (20). Indeed, aortic smooth muscle cells preloaded with EPA or DHA showed an attenuated proliferative response to serotonin and PDGF (20).

The exact molecular mechanisms of these beneficial effects are still unknown. On the molecular level it has been shown that DHA and EPA, which are dose-dependently incorporated in phospholipid fraction of vascular smooth muscle cells (21), inhibit the proliferation of vascular smooth muscle cells by modulating various steps of the signal transduction by PDGF (22). Furthermore, EPA and DHA inhibited G1/S progression, inhibited the phosphorylation of Cdk2 protein and Cdk2 kinase activity without altering the amount of cyclin E and p27(kip1) proteins (21).

In the case of human cancer cell lines, DHA has been shown to inhibit cell growth by activation of the unfolded protein response and changes in the lipid metabolism (23). Furthermore, DHA can either strengthened the cellular antioxidant defense system or lead to lipid peroxidation and oxidative stress; effects that are dependent on dose and time of supplementation (24). Finally, experiments in mouse thymocytes revealed that omega-3 PUFAs induce the release of intracellular calcium from endoplasmic reticulum stores, which in turn induces mitochondrial reactive oxygen species production finally resulting in cell death (25). This is supported by the finding that the EPA's anti-proliferative effect is blocked by the addition of anti-oxidants (26).

In addition to above described anti-proliferative mechanisms, DHA was shown to induce apoptosis in vascular smooth muscle cells through two distinct mechanisms: (1) a p38-dependent pathway that regulates PPAR-alpha and (2) a p38-independent pathway via dissipation of mitochondrial membrane potential and cytochrome c release (27).

Taken together, the exact mechanism of action of n-3 PUFA still remains unresolved and probably involves several different, simultaneously acting and overlapping pathways.

1.3. UNFOLDED PROTEIN RESPONSE

Endoplasmic reticulum (ER) is an intracellular organelle that serves as an intracellular store of Ca^{2+} ions, site of sterol and lipid synthesis and site for folding of secretory and transmembrane proteins (28). Proper protein folding is mediated by ER-resident calcium-dependent molecular chaperones such as glucose-regulated protein, 78 kDa (GRP78; also known as HSPA5), GRP94 (also known as HSP90B1) and calreticulin, which help to stabilize protein-folding intermediates (29). Additionally, the formation of disulphide bonds is mediated by protein disulphide isomerase (PDI) (29). Additional posttranslational protein modification that takes place in the ER is the covalent addition of specific oligosaccharide structures in the process termed protein glycosylation. This process also contributes to proper protein folding in the ER (29).

Proper protein folding is a sensitive process. Therefore, the cell maintains a tightly regulated environment inside the ER to mediate this process. The environment inside the ER lumen is in many respects quite different to that of the cytoplasm, in particular with respect to high calcium concentration and oxidizing conditions. Perturbation of any of these functions causes a condition termed ER stress and activates a signal transduction network termed the unfolded protein response (UPR) (28). Under normal conditions, ER lumen resident chaperon proteins bind to

transmembrane ER signaling proteins responsible for the UPR and keep them in an inactive state (29). During the accumulation of unfolded proteins inside the ER lumen, chaperons bind to unfolded proteins thereby activating ER transmembrane UPR sensors (29). These UPR initiating proteins, which have their N terminus in the lumen of the ER and their C terminus in the cytosol and thus bridge these two cellular compartments (29), set off a sequence of events that can have a profound effect on the cellular fate.

There are three crucial UPR initiating proteins: PRKR-like ER kinase (PERK; also known as EIF2AK3), inositol-requiring kinase 1 (IRE1; also known as ERN1) and activating transcription factor 6 (ATF6) (29). Together, these proteins induce signal-transduction events that ameliorate the accumulation of misfolded proteins in the ER by increasing the expression of ER chaperones, by inhibiting protein entry into the ER by arresting mRNA translation, and by accelerating the retrograde export of proteins from the ER to the cytosol for ubiquitylation and proteasome-mediated degradation (29). However, concomitant with the activation of these prosurvival adaptive pathways, there is a simultaneous activation of proapoptotic signals converging to CHOP, but also involving an IRE1-JNK pathway (30). Therefore, prolonged and unresolved ER stress in the form of activated UPR can result in cell death.

IRE1α protein is a transmembrane protein that has both a Ser/Thr kinase domain and an endoribonuclease domain (29). The endoribonuclease domain excises an intron from the X-box-binding protein 1 (XBP1) mRNA, producing a shorter splice variant that is competent for translation to produce the 41 kDa XBP1 protein, a basic leucine zipper (bZIP) family transcription factor (29). In a downstream signaling cascade, XBP1 heterodimerizes and binds to promoters of several genes involved in UPR and ERAD (29) to induce their transcription. IRE1α is required for cleavage and post-transcriptional degradation of many mRNAs that encode secreted proteins, thereby reducing the protein load on the ER (29).

PERK is a Ser/Thr protein kinase, whose autophosphorylation and kinase domain activation is initiated by oligomerization in ER membranes (29). PERK phosphorylates and inactivates eIF2α, shutting off mRNA translation and reducing the protein load on the ER (29) in addition to endoribonuclease action of IRE1α. However, certain mRNAs, including the mRNA encoding transcription factor ATF4 involved in the UPR pathway, have a selective advantage for translation under conditions in which eIF2α is phosphorylated (29).

ATF6 belongs to the bZIP family of transcription factors that activates gene transcription either as homodimer or upon heterodimerization with certain other bZIP transcription factors, including XBP1 (29). ATF6 proteins have an ER-targeting hydrophobic sequence that tethers them to ER membranes (29). Binding of GRP78 frees ATF6 proteins to translocate to the Golgi, where resident proteases cleave at a juxtamembrane site, releasing these transcription factors into the cytosol and allowing them to migrate into the nucleus to regulate gene expression (29). Known or suspected target genes of ATF6α include GRP78, PDI and ER degradation-enhancing α-mannosidase-like protein 1 (EDEM1) (29). Furthermore, ATF6α induces the transcription of XBP1 mRNA, which is spliced by the endoribonuclease activity of IRE1 (29). This part of the ATF6 mediated response belongs to adaptive and prosurvival effects since it leads to increased ER chaperone activity and degradation of misfolded proteins (29). However, ATF6 and ATF4 mediated pathways can also activate another transcription factor, CHOP (also known as GADD153) (30). Activation of this arm of UPR leads to ER stress triggered apoptosis, which is executed through ER-specific initiator caspases (caspase-12 in many species and its equivalent in humans) and downstream caspases 9 and 3 (30).

Since the ER lumen is maintained in an oxidized state, ER can serve as a source of ROS during UPR. Oxidizing environment of ER is maintained by oxidoreductase Ero1-L which transfers oxidizing equivalents to its substrate PDI (30). Ero1 is an oxygen-consuming enzyme that is able to generate ROS and expression of beta

isoform is induced in UPR (30) thereby being a possible link between ER and oxidative stress.

2. MATERIALS AND METHODS

2.1. CELLS

Human pulmonary artery smooth muscle cells (hPASMC) were isolated from pulmonary arteries obtained from patients undergoing surgery for lung cancer without a history of pulmonary vascular disease or arterial hypoxemia, as described previously (31). Briefly, the adventitia from small arteries with diameters of less than 1 mm was carefully removed under microscopic guidance and media pieces less than 1 mm^3 were placed into flasks with one drop of culture medium supplemented with 20% fetal calf serum (FCS). The study protocol for tissue donation was approved by the Institutional Review Board of the Medical University of Graz in accordance with the national law, and with the guidelines on Good Clinical Practice/International Conference on Harmonization. Written informed consent was obtained from each individual patient. Cells were grown in medium containing 5% FCS and growth factors (Lifeline Cell Technology, Frederick, MD, USA) and used between passages 2 and 5. Purity was checked by characteristic appearance in phase-contrast microscopy indirect immunofluorescence staining for alpha smooth muscle actin, smooth muscle myosin heavy chain and lack of von Willebrand factor staining.

2.2. CHEMICALS

Antibodies against human phospho eIF2alpha, total eIF2alpha, cyclin D1, p21, alpha tubulin, cleaved caspase-3 Alexa 488 and anti-rabbit horseradish peroxidase-conjugated secondary antibody were obtained from Cell Signaling (Beverly, MA, USA). Taq Polymerase (Solis Biodyne, Tartu, Estonia), 10x PCR Buffer and dNTP mix (Promega, Madison, WI). DHA, DMSO, ethanol, $CaCl_2$, KCl, $MgCl_2$, NaCl, Hepes, EGTA, glucose, 4-hydroxy-Tempo (Tempol), BSA, Triton X-100 and propidium iodide were bought from Sigma (Steinheim, Germany). Tween

20 was bought from Bio-Rad (Hercules, CA, USA). BAPTA-AM (cell permeable Ca^{2+} chelator) and RU360 (mitochondrial calcium uptake inhibitor) were obtained from Merck Biosciences (Nottingham, UK). [methyl-^{3}H]thymidine was obtained from Perkin Elmer (Waltham, MA, USA). DHA was reconstituted in ethanol, aliquoted in glass vials under argon and stored at -80°C until use. Vehicle controls contained a maximum of 0.05% ethanol or 0.1% DMSO.

2.3. PROLIFERATION

Cells plated in 24-well plates were grown for 3 days with DHA or vehicle control. At the end of the experiment, cells were harvested by trypsinization, centrifuged and resuspended in PBS. An aliquot of the cell suspension was taken for cell number count. Number of viable and total cells was determined by Casy machine (Schärfe System, Reutlingen, Germany), a pulse area-based technology for cell counting and viability testing.

2.4. THYMIDINE INCORPORATION

Cells were plated in 96-well plates and incubated with compounds and 2 µCi/well [methyl-^{3}H]thymidine overnight. Cells were harvested (Perkin Elmer Harvester) and transferred to glass fiber plates (UniFilter-96 GF/C, PerkinElmer Life Sciences) and radioactivity measured in the scintillation counter (1450 Microbeta Trilux Liquid Scintilation and Luminescence Counter, Wallac).

2.5. APOPTOSIS AND CELL CYCLE MEASUREMENTS

Cleaved caspase-3 was determined in cells that were incubated for indicated time intervals with DHA in 24-well plates, harvested by trypsinization, washed in PBS, fixed 10 minutes at 37°C in 2% formaldehyde and permealibized in ice-cold

methanol for 30 minutes. Cells were then washed in PBS with 0.5% FCS, incubated with cleaved caspase-3 antibody at room temperature for 45 minutes, washed, resuspended in PBS and measured immediately on FACS Calibur (BD Biosciences, Franklin Lakes, NJ, USA) flow cytometer.

TUNEL assay for detection of apoptotic cells was performed on cells cultured and treated in glass chamber slides. Cells were washed with PBS, fixed with 4% paraformaldehyde for 1 hour at room temperature and permeabilized on ice with 0.1% Triton X-100 in 0.1% Na-citrate solution. Afterwards, cells were incubated with reagents from an in situ cell death detection kit according to manufacturer's instruction (Roche, Mannheim, Germany).

Cell cycle was determined flow cytometrically by staining cells with propidium iodide (PI). Cells were harvested by trypsinization, washed with PBS, incubated at room temperature for 20 minutes with 50 μg/mL PI in 0.1% Na-acetate with 0.1% Triton X-100 and measured immediately on FACS Calibur flow cytometer. Acquired data were analyzed with CellQuest Pro software (BD Biosciences, Franklin Lakes, NJ, USA).

2.6. ROS AND MITOCHONDRIAL MEMBRANE POTENTIAL MEASUREMENTS BY FLOW CYTOMETRY

ROS production was determined using 2', 7'-dichlorohihydrofluorescein diacetate (H_2DCFDA) dye (Biotium, Hayward, CA; USA). Cells grown in full medium with 5% FCS in 24-well plates were loaded with 10 μM H_2DCFDA for 30 minutes. Thereafter, medium was replaced with a fresh medium containing vehicle or DHA, followed by incubation for indicated time periods and flow cytometric measurements of ROS. For 24 h-time point cells were incubated with vehicle or DHA for 23.5 hours followed by labeling with 10 μM H_2DCFDA for 30 minutes before flow cytometric measurements of ROS. In some experiments, 5 μM BAPT-AM and 10 μM RU360 were added during both labeling with H_2DCFDA and

incubation with vehicle or DHA. To address the role of ROS scavenger Tempol, cells were pre-incubated with Tempol (150 µM) or vehicle (DMSO) for 2 hours (90 minutes before and during 30 minutes-labeling with H_2DCFDA). Thereafter, cells were exposed to DHA in the presence or absence of Tempol for 3 hours. At the end of the experiment, cells were harvested by trypsinization, washed and resuspended in PBS, followed by flow cytometry.

For ROS measurements in calcium- and calcium free- buffer, cells were first loaded with H_2DCFDA in full medium with 5% FCS for 30 minutes. Then, cells were washed with calcium- or calcium free-buffer and incubated with vehicle or DHA in the respective buffers for 1 hour, followed by ROS measurements. Calcium containing buffer contained 2 mM $CaCl_2$, 138 mM NaCl, 1 mM $MgCl_2$, 5 mM KCl, 10 mM Hepes, 10 mM glucose, 5% FCS; pH 7.4. Calcium free- buffer lacked $CaCl_2$ but contained 1 mM EGTA.

Mitochondrial ROS production was measured using MitoSOX Red (Invitrogen, Darmstadt, Germany) a fluorogenic dye. Cells were loaded with 1 µM MitoSOX Red for 30 minutes, in the absence or presence of RU360 (10 µM) followed by incubation with vehicle or DHA in the presence or absence of RU360 for 1 hour. At the end of the experiment, cells were harvested by trypsinization, washed and resuspended in PBS followed by flow cytometry.

$\Delta\Psi_m$ was measured using Mito ID Membrane Potential Detection Kit (Enzo Life Sciences, Lorrach, Germany). Cells were incubated for indicated time with DHA, then harvested by trypsinization, washed, and incubated at room temperature for 15 minutes with reagent followed by flow cytometry. Loss of MMP is observed as a decrease in orange and increase in green fluorescence. Results are represented as a change in ratio of two fluorescence means that correlates to changes in $\Delta\Psi_m$.

2.7. ARRAY CONFOCAL LASER SCANNING MICROSCOPY

High resolution imaging of cells loaded with both 1µM MitoSOX™ Red and 0.5 µM MitoTracker® Green for 30 minutes, followed by incubation with vehicle or DHA was performed using an array confocal laser scanning microscope (ACLSM). The ACLSM was built on an inverse, fully automatic microscope (Axio Observer.Z1 from Zeiss, Göttingen, Germany) that was equipped with a 100x objective (Plan-Fluor 100x/1.45 Oil, Zeiss), a Nipkow-based confocal scanner unit (CSU-X1, Yokogawa Electric Cooperation, Tokyo, Japan), a motorized filter wheel (CSUX1FW, Yokogawa Electric Cooperation) on the emission side, and an acousto optic tunable filter (AOTF)-based laser merge module for laser lines 405 nm, 445 nm, 473 nm, 488 nm, 515 nm, and 561 nm (Visitron Systems, Pucheim, Germany). Emission was acquired with a charged-coupled device (CCD) camera (CoolSNAP-HQ, Photometrics, Tucson, USA). All devices were controlled by VisiView Premier acquisition software (Visitron Systems). MitoSOX™ Red and MitoTracker® Green were alternatively excited at 561 nm and 488 nm and fluorescence emission light was collected at 630/75 nm and 525/40 nm, respectively. Image analysis (colocalization analysis) was performed using MetaMorph® Software 7.7 (Molecular Devices, Sunnyvale, California, USA).

2.8. ADENINE NUCLEOTIDE ANALYSIS

Adenine nucleotides were analyzed as reported previously (32,33) with some modifications. Separation was performed on a Hypersil ODS column (5 µm, 250 x 4 mm ID), using a L2200 auto sampler, two L-2130 HTA pumps, and a L2450 diode array detector (all from VWR Hitachi). The wavelength for detection of adenine nucleotides was set at 254 nm. EZchrom Elite (VWR) was used for data acquisition and analysis. After trypsinization and mild centrifugation (supernatant discarded), the cellular proteins were precipitated with 250 µL of perchloric acid (0.4 mol/L, 4°C). After centrifugation (12,000 x g), 100 µL of the supernatant were neutralized with 10-12 µL of potassium carbonate (2 mol/L, 4°C). The supernatant obtained after centrifugation was used for HPLC analysis (injection volume: 40

µL). The pellets of the acid extract were dissolved in 0.5 mL of sodium hydroxide (0.1mol/L) and used for protein determination (BCA Assay; Pierce).

2.9. MASS SPECTROMETRIC DETERMINATION OF PHOSPHOLIPID AND TRIGLYCERIDE SPECIES

Cells grown in 6-well plates were treated with DHA or vehicle for 20 hours followed by extraction of cellular lipids according to Bligh and Dyer (34) followed by HPLC and MS as described previously (35,36).

2.10. MEASUREMENT OF INTRACELLULAR CALCIUM

Intracellular calcium was measured as described previously (37). Cells were trypsinized and loaded with 2 µM fura-2/AM for 45 minutes. After washing, cells were resuspended either in calcium buffer (138 mM NaCl, 1 mM MgCl2, 5 mM KCl, 10 mM Hepes, 10 mM Glucose, pH 7.4) or EGTA buffer (1 mM EGTA, 138 mM NaCl, 1 mM MgCl2, 5 mM KCl, 10 mM Hepes, 10 mM Glucose, pH 7.4). The ratio of fura-2 fluorescence intensity at the 2 excitation wavelengths (340 nm/380 nm ratio) was monitored fluorometrically in a stirring cuvette before and after the injection of vehicle or 10 µM DHA. Values obtained with vehicle were subtracted from those obtained with DHA.

2.11. WESTERN BLOT

Cells were washed once with ice-cold PBS and lysed in M-PER Mammalian Protein Extraction Reagent (Thermo Scientific, Rockford, IL, USA) containing protease and phosphatase inhibitors (Roche, Mannheim, Germany). Equal amounts of proteins were loaded per lane and analyzed by SDS-PAGE (10%) and subsequent immunoblotting. Nitrocellulose membrane (Bio-Rad) was blocked in

5% milk in Tris-buffered saline (TBS) with 0.1% Tween-20 and incubated overnight at 4°C with indicated primary antibody (1:1000 in 5% BSA). Thereafter, membranes were washed and incubated with HRP-labeled secondary antibody (1:5000 in 1% milk) and developed with SuperSignal West Pico or SuperSignal West Femto Substrate (Thermo Scientific, Rockford, IL, USA). Membranes were stripped using Restore Plus Western Blot Stripping Buffer (Thermo Scientific, Rockford, IL, USA).

2.12. QUANTITATIVE REAL-TIME PCR (QRT-PCR)

Isolation of RNA and qRT-PCR was performed as described (36). Isolation of RNA from cells was performed using peqGOLD Total RNA isolation kit (PeqLab, Erlangen, Germany). Isolation of RNA from tissue was performed by phenol/chloroform/guanidinisothiocyanate method using peqGOLD TriFast Kit (PeqLab, Erlangen, Germany).

Total RNA was reverse transcribed using iScript kit (BioRad, Hercules, CA, USA) according to the manufacturer's instructions. Real-time quantitative PCR was performed using QuantiFast SYBR PCR kit (Qiagen, Hilden, Germany) using a LightCycler 480 (Roche, Mannhein, Germany).

mRNA levels of HSPA5 (Primer Assay QT00096404), cyclin D1 (QT00495285) and p21 (QT00062090) were normalized to human beta-2-microglobulin (QT01665006) and expressed as relative ratio ($\Delta\Delta$Ct).

Gene symbol : gene name - species	**QuantiTect Primer Assay (Qiagen)**
p21: p21 Human	QT00062090
ERO1L: ERO1-like (S. cerevisiae) - Human	QT00096551
Ero1l : ERO1-like (S. cerevisiae) - Mouse	QT00149863

HSPA5 : heat shock 70kDa protein 5 (glucose-regulated protein, 78kDa) - Human	QT00096404
Hspa5 : heat shock protein 5 - Mouse	QT00172361
B2M : beta-2-microglobulin - Human	QT00088935
B2m : beta-2 microglobulin - Mouse	QT01149547
Cpt1a : carnitine palmitoyltransferase 1a, liver - Mouse	QT00106820
Angptl4 : angiopoietin-like 4 - Mouse	QT00139748
Fabp5 : fatty acid binding protein 5 - Mouse	QT01743770
Cd36 : CD36 antigen - Mouse	QT01058253
Apoe : apolipoprotein E - Mouse	QT01043889
Aldh3a2 : aldehyde dehydrogenase family 3, subfamily A2 - Mouse	QT00157997
Pdk4 : pyruvate dehydrogenase kinase, isoenzyme 4 - Mouse	QT00157248
Plin2 : perilipin 2 - Mouse	QT00101045
Pparg : peroxisome proliferator activated receptor gamma - Mouse	QT00100296
Ppard : peroxisome proliferator activator receptor delta - Mouse	QT00166292
Hmox1 : heme oxygenase 1 - Mouse	QT00159915

HMOX1 : heme oxygenase (decycling) 1 - Human	QT00092645
ERO1LB : ERO1-like beta - Human	QT00050456
Ero1lb : ERO1-like beta (S. cerevisiae) - Mouse	QT01744099

Table 3. List of used primers.

All samples were assayed in duplicates and the average value was used for quantification.

2.13. DETECTION OF XBP-1 SPLICE VARIANT

Forward (CCTTGTAGTTGAGAACCAGG) and reverse (GGGGCTTGGTATATA TGTGG) primers for XBP-1 PCR were custom synthesized by Invitrogen (Darmstadt, Germany). PCR amplification program consisted of 40 cycles each containing 3 steps: 95°C, 58°C and 72°C (each 1 minute). Electrophoretic separation of resulting products was performed on 3% agarose gel in 0.5x TAE buffer at 30V for 6 hours. Unspliced XBP-1 product had a size of 422 bp and spliced variant had a size of 396 bp.

2.14. ANIMAL STUDY

Animal experiments were approved by the Austrian Ministry of Education, Science and Culture according to the regulations for animal experimentation. Fifty C57BL/6 male mice 18 weeks of age (Himberg, Austria) were used for the experiment. At the beginning of experiment, mice were randomized to 3 groups and fed for the duration of the experiment with 3 different diets: 5% saturated fat (normal, chow

diet), 21% omega-3 PUFA with 2% saturated fat (fish oil diet), 23% saturated fat (corn oil). Oil diet was reapportioned to 70 g packages filled with argon and stored at -20°C till use. Detailed food composition (ssniff Spezialdiäten, Soest, Germany) was as given in Table 4:

crude protein	17.5%	vitamin A	4000 IE/IU/kg
crude fat	23.1%	vitamin D3	1000 IE/IU/kg
crude fiber	5.0%	vitamin E	75 mg/kg
crude ash	3.3%	vitamin K3	4 mg/kg
starch	32.7%	vitamin C	--
sugar	13.5%	copper	11 mg/kg

Table 4. Mouse diet composition.
Fish and corn oil diets were both isocaloric (19.6 MJ ME/kg).

Mice were first pre-fed for 2 weeks and then put in hypoxia for 5 weeks:

- 5 mice held 7 weeks in normoxia and fed chow diet
- 5 mice held 7 weeks in normoxia and fed fish diet
- 5 mice held 7 weeks in normoxia and fed corn oil diet
- 7 mice held 2 weeks in normoxia and then 5 weeks in hypoxia, fed chow diet
- 14 mice held 2 weeks in normoxia and then 5 weeks in hypoxia, fed fish oil diet
- 14 mice held 2 weeks in normoxia and then 5 weeks in hypoxia, fed corn oil diet

Mice were maintained for 5 weeks in normoxia or 10% normobaric hypoxia in ventilated chambers. Oxygen concentration was monitored and maintained continuously using the OxyCycler system (BioSpherix, Lacona, NY, USA). Cages were opened for husbandry once per week.Food consumption was measured every day for the first 5 weeks, and body mass every week for the duration of the experiment.

At the end of experiment, mice were sacrificed by cervical dislocation. Heart, lungs and liver were collected for further analysis. Hearts without atria were collected for weight determination of right ventricle to left ventricle and septum (Fulton index). Left lung half was formalin-fixed and paraffin-embedded, while right lung half was snap frozen and stored in liquid nitrogen.

2.15. STATISTICS

Data are given as mean±SEM. Statistical analyses were performed in GraphPad Prism 5 using the paired t test, for experiments comparing 2 groups; and ANOVA Kruskal-Wallis with the Dunn's multiple comparison post-test, for experiments comparing 3 or more groups. $P<0.05$ was considered statistically significant

.

3. RESULTS

3.1. DHA INHIBITS HUMAN PULMONARY ARTERY SMOOTH MUSCLE CELL (HPASMC) PROLIFERATION

DHA has a known anti-proliferative effect on both tumor cell lines and primary cells, including smooth muscle cells. Therefore, the DHA effect on the proliferation of primary human smooth muscle cells (hPASMC) was tested under different conditions and with 2 independent methods. First, hPASMC were incubated with a range of different DHA concentrations, chosen based on published in vitro data. Cells were incubated with DHA in fully supplemented medium and exposed to either normoxia or hypoxia. After 3 days of incubation, proliferation was determined by cell counting (Fig. 1A) and ^{3}H-thymidine incorporation (Fig. 1B). DHA in both cases dose-dependently inhibited hPASMC proliferation. Furthermore, DHA showed the same effect under both normoxia and hypoxia, though the overall hPASMC proliferation in hypoxia was lower when compared to normoxia.

The effect of hypoxia alone on hPASMC proliferation was further investigated. Time-course experiment showed a clearly decreased proliferation of hPASMC under hypoxia (1% oxygen) in comparison to normoxia (20% oxygen) evident already at day 2 (Fig. 2).

Platelet-derived growth factor (PDGF) is a potent mitogen for hPASMC and, in addition to hypoxia, is an additional factor involved in development and progression of pulmonary vascular remodeling. Since serum and supplements for normal culturing of hPASMC contain large amounts of various growth factors, including PDGF, cells for this experiment were exposed to starvation medium – medium containing only 0.1% serum. The concentration of serum proteins that bind DHA was significantly lower in the starvation medium when compared to the normal, fully supplemented medium, effective –concentration of free, unbound DHA was higher. Due to this reason, concentration of DHA that was applied to

cells was lowered to 25 μM. As expected, PDGF increased hPASMC proliferation measured by cell number counting and DHA inhibited both PGDF-induced and basal level of hPASMC proliferation (Fig. 3).

In addition to DHA, EPA is another omega-3 fatty acid that is present both naturally and in nutritional supplements. EPA also dose-dependently inhibited hPASMC proliferation determined by cell counting (Fig. 4) albeit to a lesser degree when compared to DHA.

Similarly, α-linolenic acid is also a member of omega-3 fatty acids with described positive cardiovascular effects. However, also in this case, DHA showed a more potent effect on hPASMC proliferation than α-linolenic acid (Fig. 5). In order to see if this effect is specific only for omega-3 fatty acids, arachidonic acid, as a representative of omega-6 fatty acids, was also tested for its ability to inhibit hPASMC proliferation. Obtained results (Fig. 5) show that both arachidonic acid is capable to inhibit hPASMC proliferation, albeit with a lower efficiency when compared to DHA.

DHA dose-dependent proliferation studies were repeated on hPASMC isolated and cultured from 5 different donors (Fig. 6A and B). Based on these results and literature reports on plasma DHA concentration in humans, we used DHA at 100 μM in all subsequent experiments, which showed potent and consistent effect through all independent experiments.

One mechanism of decreased proliferation could be blocked progression thorough cell cycle. The observed inhibitory action of DHA on cell proliferation was accompanied by an increased percentage of cells in G1 phase of the cell cycle (Fig. 6C). Protein expression level of cyclin D1, a positive regulator of cell cycle progression, was significantly decreased in DHA-treated cells (Fig. 6D and E). Protein expression level of p21, a negative regulator of cell cycle progression, was unaltered upon DHA treatment (Fig. 6D and F). Taken together, the data supports the finding of DHA-induced G1 cell cycle arrest in hPASMC.

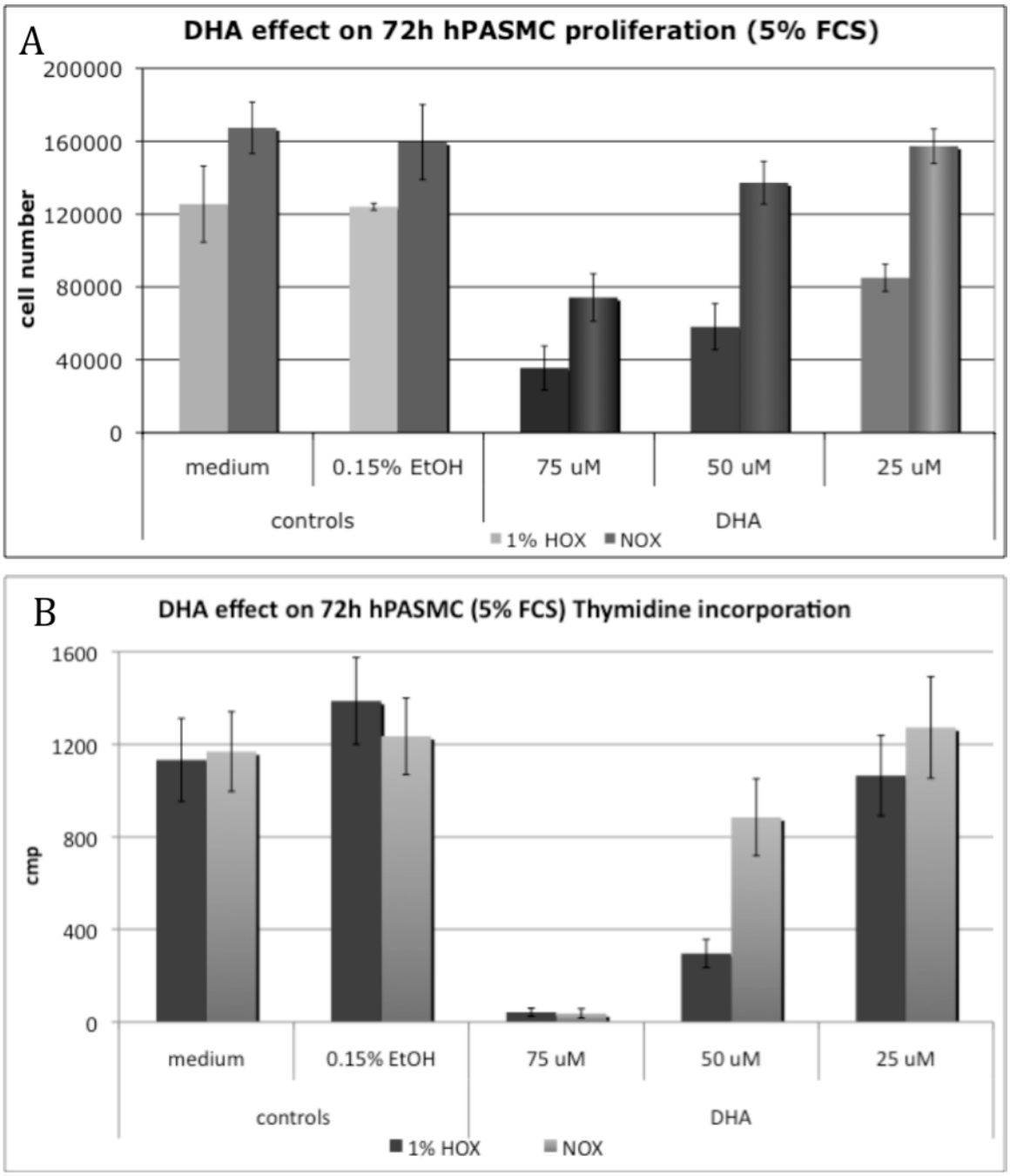

FIG. 1. DHA dose-dependently inhibits hPASMC proliferation. (**A**) Number of viable cells was determined after 3 days of incubation with indicated concentrations of DHA. (**B**) [^{3}H]Thymidine incorporation was measured after overnight incubation with DHA and results expressed as count per minute. Data are given as mean±SEM of one representative measurement.

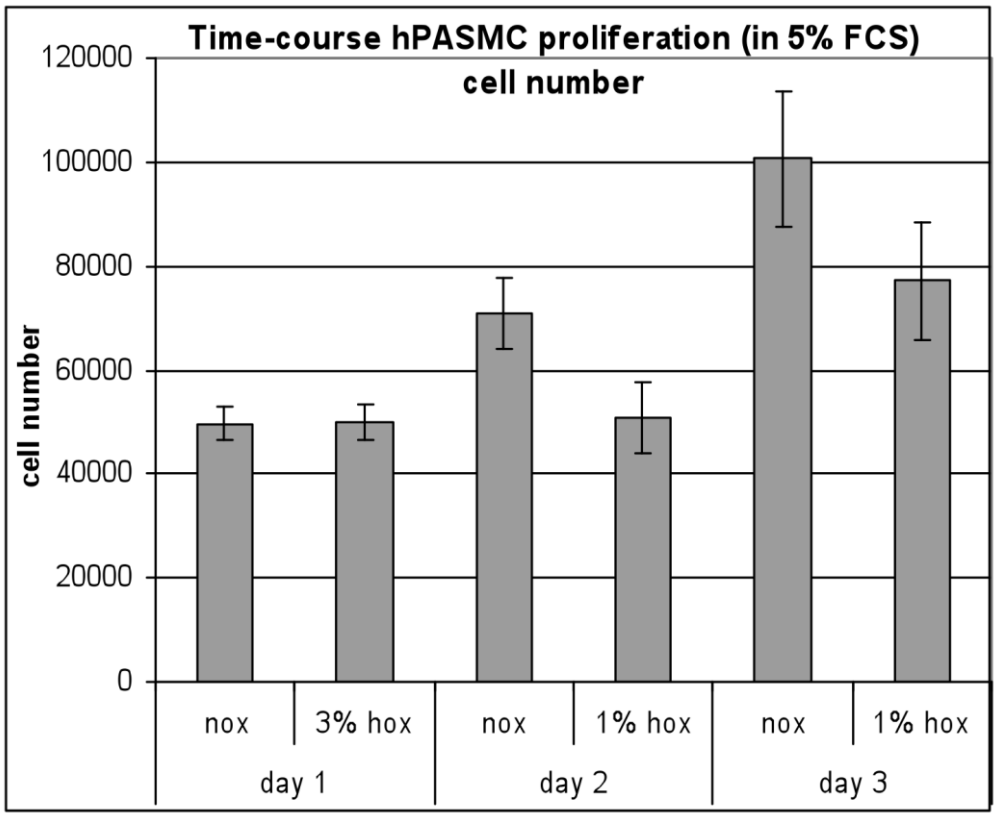

FIG. 2. Hypoxia inhibits hPASMC proliferation. Number of viable cells was determined after 1, 2 and 3 days of incubation in fully supplemented medium under normoxia or hypoxia (1% oxygen). Data are given as mean±SEM of one representative measurement.

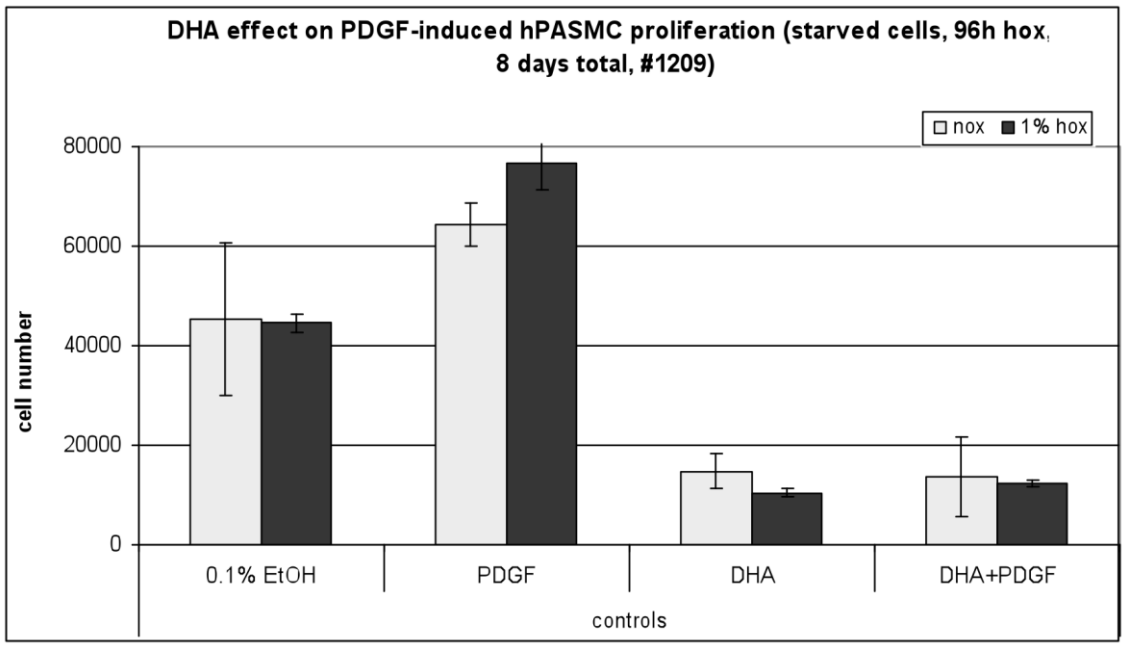

FIG. 3. DHA inhibits PDGF-induced hPASMC proliferation. Number of viable cells was determined after 3 days of incubation with 10 ng/mL PDGF and 25 μM DHA. Data are given as mean±SEM of one representative measurement.

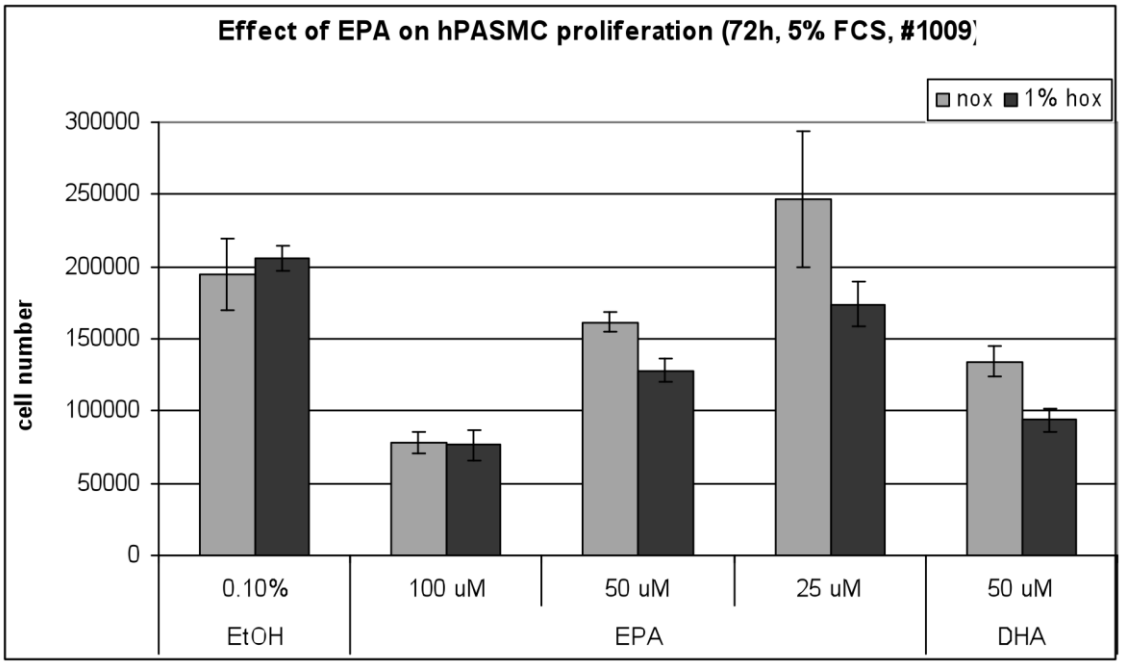

FIG. 4. EPA dose-dependently inhibits hPASMC proliferation. Number of viable cells was determined after 3 days of incubation with indicated concentrations of EPA. For comparison of effect, DHA was used in a single effective concentration. Data are given as mean±SEM of one representative measurement.

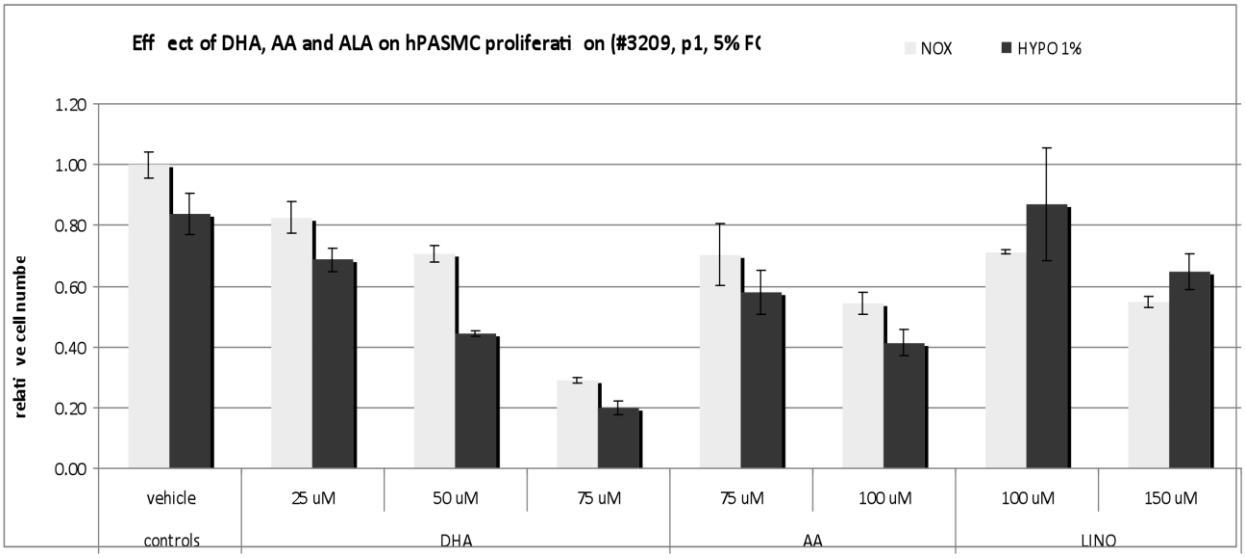

FIG. 5. Polyunsaturated fatty acids dose-dependently inhibit hPASMC proliferation. Number of viable cells was determined after 3 days of incubation with indicated concentrations of DHA, arachidonic acid (AA) and α-linolenic acid (LINO). Results are expressed relative to vehicle control. Data are given as mean±SEM of one representative measurement.

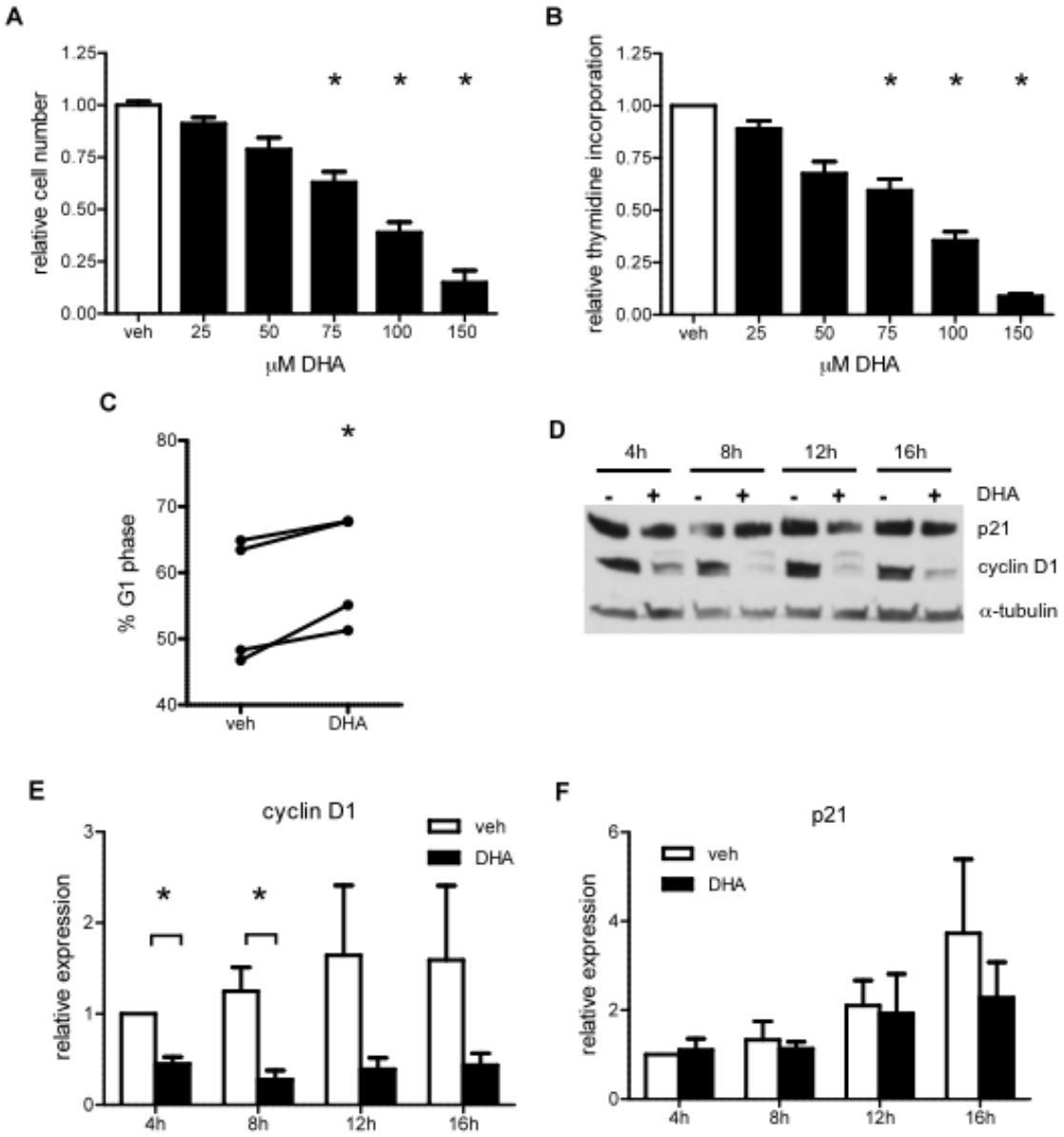

FIG. 6. DHA dose-dependently inhibits hPASMC proliferation. (**A**) Number of viable cells was determined after 3 days of incubation with indicated concentrations of DHA. Results are expressed relative to vehicle control (n=5). (**B**) [^{3}H]Thymidine incorporation was measured after overnight incubation with DHA. Results are expressed relative to vehicle control (n=5). (**C**) Cells were treated with 100 μM DHA for 12 hours and analyzed by flow cytometry for DNA content. Cell cycle distribution in G1 phase is expressed as percentage of total cells (n=4). (**D**) Cells were treated with 100 μM DHA and representative time course results of p21 and cyclin D1 Western blots are shown. (**E**) and (**F**) Densitometry evaluation of

Western blot data. Signals were normalized to a-tubulin and expressed relative to 4h vehicle (veh) control (n=4). Data are given as mean±SEM of at least 4 independent experiments. *P<0.05 vs. corresponding veh control group.

3.2. DHA INDUCES THE UNFOLDED PROTEIN RESPONSE (UPR) IN HPASMC

In order to investigate in more detail the molecular mechanisms of DHA-induced cell cycle arrest, I focused on the possible activation of the unfolded protein response in DHA-treated hPASMC. UPR is characterized by activation of three sensor pathways originating from endoplasmatic resticulum (ER). In order to test the activation of these pathways and thus the induction of UPR, three commonly used UPR markers were measured in DHA-treated hPASMC.

The levels of HSPA5 (Bip) mRNA were significantly increased in DHA-treated cells, compared to vehicle treated control cells (Fig. 7A). Furthermore, the phosphorylation level of eIF-2a was significantly increased in DHA-treated cells (Fig. 7B and C). Finally, splicing of XBP-1 mRNA was induced upon incubation with DHA (Fig. 7D).

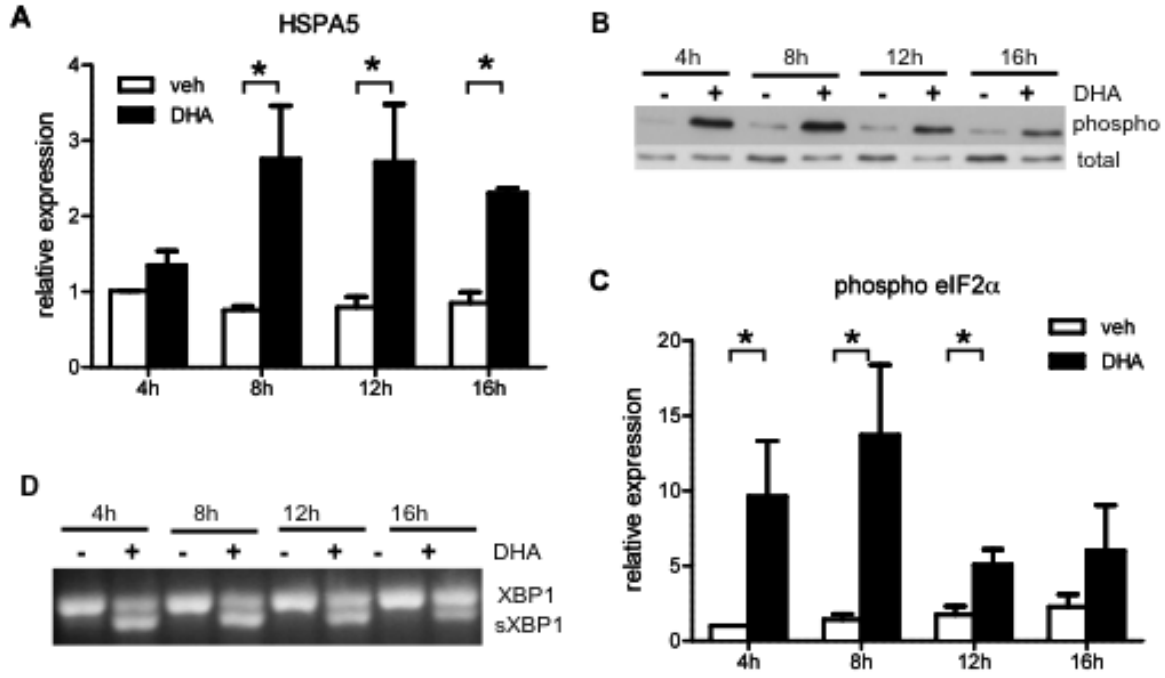

FIG. 7. DHA induces UPR in hPASMC. (**A**) Quantitative RT-PCR measurement of HSPA5 gene expression (n=4). (**B**) Representative Western blot detection of phosphorylated eIF-2a. Total eIF-2a served as loading control. (**C**) Densitrometric evaluation of eIF-2a phospholylation (n=4). (**D**) Representative PCR detection of XBP-1 splice variant. Data are given as mean±SEM. *P<0.05 vs corresponding vehicle (veh) control group.

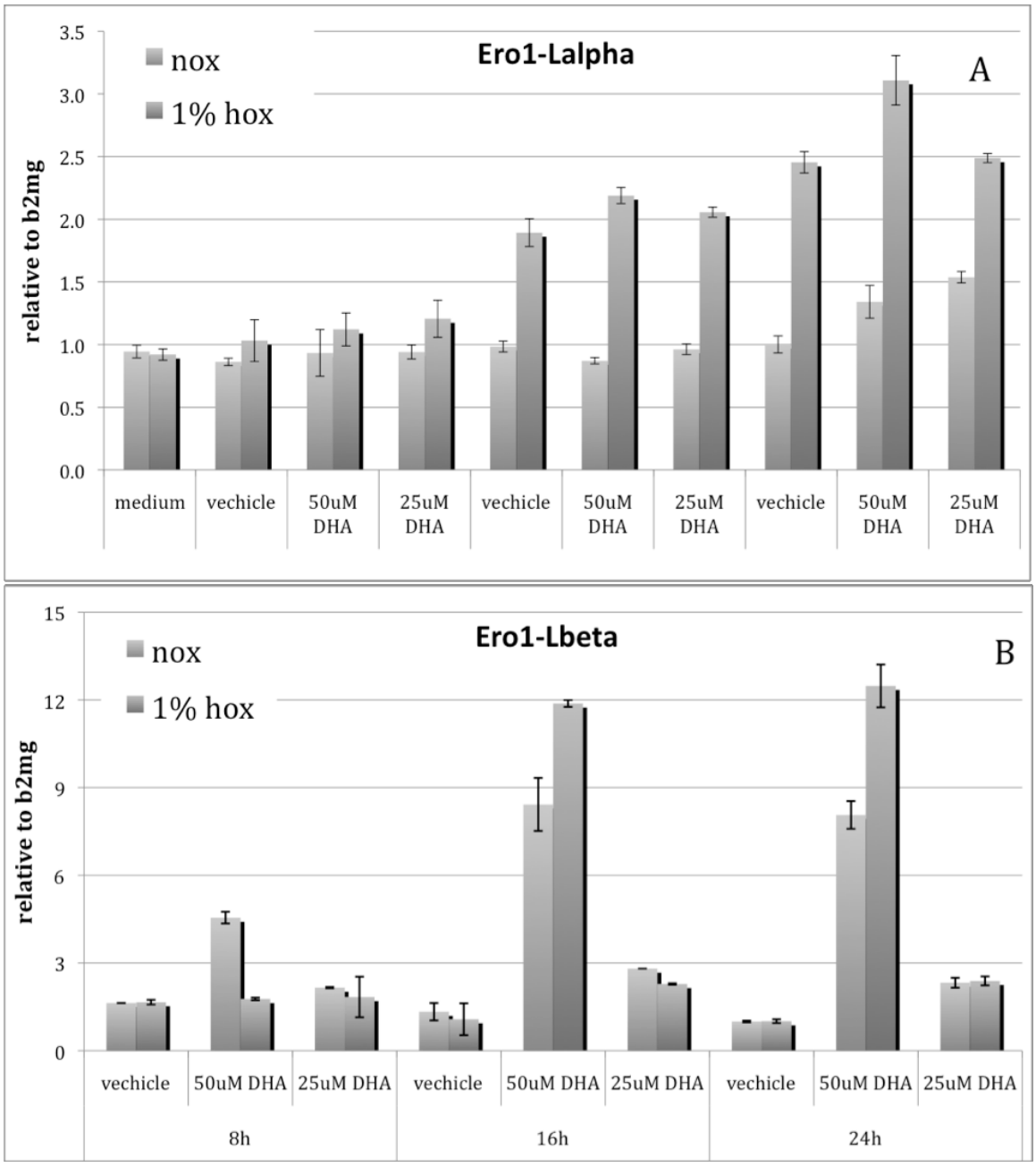

FIG. 8. Effect of DHA on expression of hypoxia and UPR marker genes in hPASMC. (**A**) Quantitative RT-PCR measurement of Ero1-Lα gene expression (**B**) Quantitative RT-PCR measurement of Ero1-Lβ gene expression. Data are given as mean±SEM of one representative measurement.

Finally, we observed an isoform specific increase in the gene expression of oxidoreductase Ero1-L under different stress conditions. Whereas hypoxia

increased expression of hypoxia-responsive Ero1-Lα isoform in both DHA-treated and untreated cells (Fig. 8A), gene expression of Ero1-Lβ isoform was dose-dependently increased only in DHA-treated cells (Fig. 8B).

Taken together, the results show the activation of UPR in DHA-treated cells and indicate this as a possible mechanism of DHA-induced cell cycle arrest.

3.3. DHA ALTERS THE LIPID PROFILE OF HPASMC

Since alterations in cellular lipid composition might be responsible for ER stress and UPR, phospholipid- and triglyceride- profiling of DHA- and vehicle-treated cells was performed by mass spectrometry. Both phosphatidylcholine (PC) species 38:6, 40:6 and 40:7 (Fig. 9A) as well as phosphatidylethanolamine (PE) species 40:6 and 40:7 (Fig. 9B) were markedly enriched in DHA treated cells compared with vehicle treated control cells. These phospholipids contain omega-3 fatty acid molecules in their structure. The observed increase in PC and PE species that contain DHA was accompanied by a marked decrease in several phospholipid species that lack DHA (Fig. 9A and B). Additionally, there was a significant enrichment of lysophospholipids with DHA containing species and a corresponding decrease in species containing other fatty acids such as 18:1 or 20:4 (Fig. 9C, D).

DHA was also efficiently incorporated into triglycerides (TG) as reflected by the increase in TG species containing long chain polyunsaturated fatty acids including DHA (not shown).

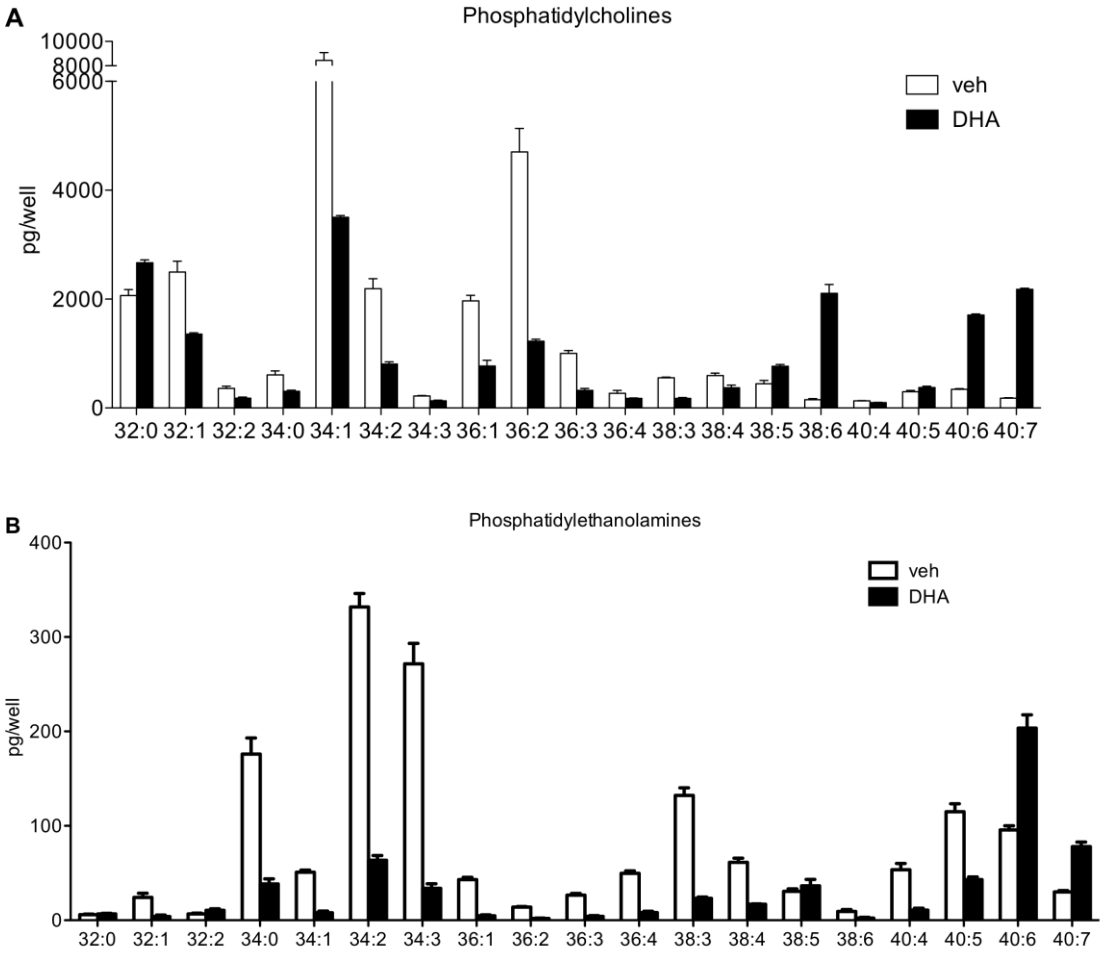

FIG. 9. DHA alters cellular phospholipid composition. hPASMC were incubated with 100 μM DHA for 20 hours followed by lipid extraction and mass spectrometric analysis of phospholipid species. (**A**) DHA-induced alterations in cellular phosphatidylcholine profile. (**B**) DHA-induced alterations in cellular phosphatidylethanolamine profile.

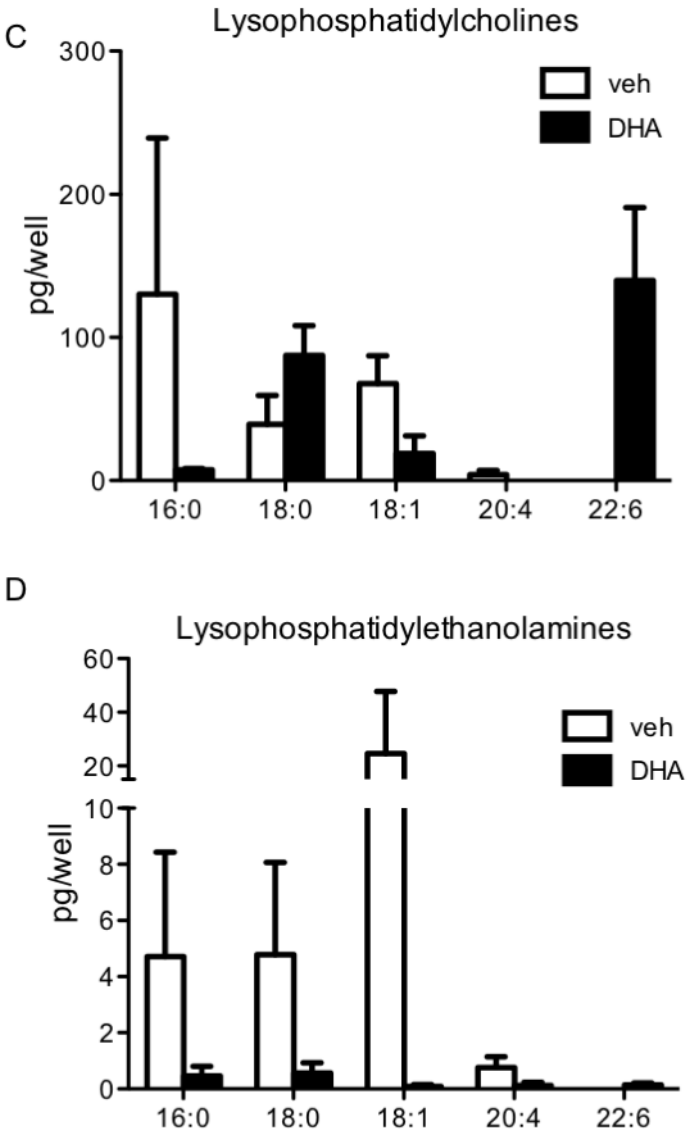

FIG. 9. DHA alters cellular phospholipid composition. hPASMC were incubated with 100 μM DHA for 20 hours followed by lipid extraction and mass spectrometric analysis of phospholipid species. (**C**) DHA-induced alterations in cellular lysophosphatidylcholine profile. (**D**) DHA-induced alterations in cellular lysophosphatidylethanolamine profile. Experiments were done by Monika Riederer and by ZMF Mass Spectrometry Core Facility.

3.4. DHA-INDUCES OXIDATIVE STRESS IN HPASMC: IMPACT ON CELL PROLIFERATION AND UPR

Due to the high number of unsaturated bonds, DHA might have a pro-oxidative action and oxidative stress might, in addition to disturbed lipid composition, lead to development of UPR. Upregulation of heme oxygenase 1 (HO-1) occurs frequently under various stress conditions. Indeed, HO-1 gene expression was significantly and very early upregulated in hPASMC exposed to DHA (Fig. 10).

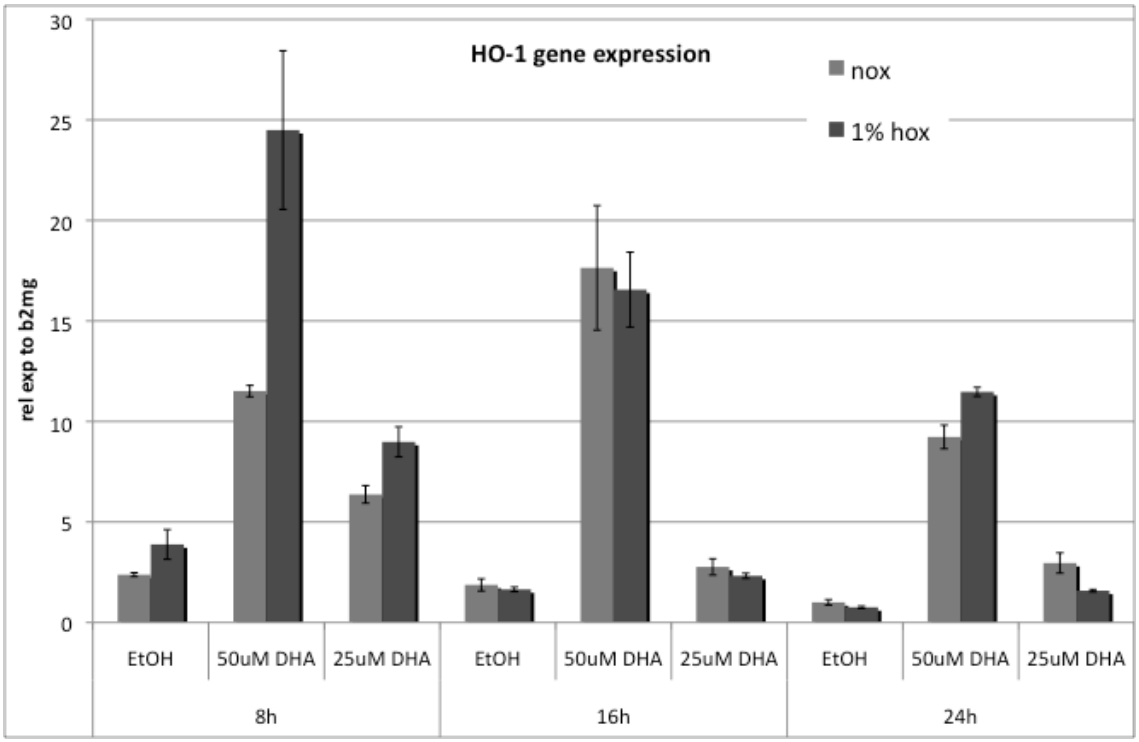

FIG. 10. Effect of DHA on expression of heme oxygenase-1 (HO-1) in hPASMC. Quantitative RT-PCR measurement of HO-1 gene expression. Data are given as mean±SEM of one representative measurement.

To further examine whether DHA-induced oxidative stress is implicated in the promotion of ER stress, we measured intracellular reactive oxygen species (ROS) production in DHA-treated cells. We observed a rapid increase in ROS production under DHA treatment, starting already after 10 minutes incubation, with a

maximum after 1 and 3 hours, followed by a decreasing trend after 5 hours and similar levels in DHA and vehicle treated cells after 24 hours (Fig. 11A). DHA-induced ROS was significantly decreased by preincubation with the free radical scavenger Tempol (Fig. 11B). Tempol markedly recovered both DHA-mediated inhibition of cell proliferation (Fig. 11C) and cyclin D1 protein expression (Fig. 11D) and diminished DHA-induced phosphorylation of eIF-2a (Fig. 11E).

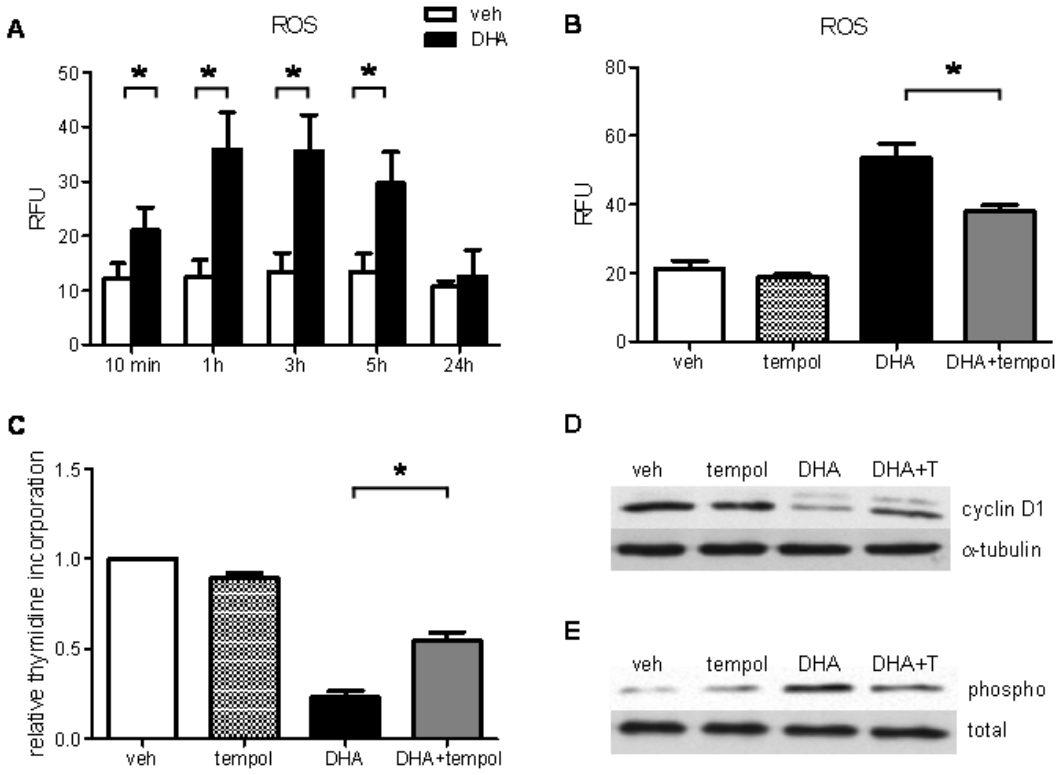

FIG. 11. Free radical scavenger Tempol attenuates DHA-induced oxidative stress, UPR and improves cell proliferation. (**A**) Cells were loaded with 10 μM H_2DCFDA for 30 minutes followed by exposure to vehicle or DHA (100 μM) for indicated time periods up to 5 hours, followed by flow cytometry. For 24 h-time point cells were incubated with veh or DHA for 23.5 hours, then loaded with H_2DCFDA for 30 minutes in the presence of veh or DHA, followed by flow cytometry (**B**) Cells were pre-incubated with Tempol (150 μM) or veh (DMSO) for 2 hours (90 minutes before loading and during 30 minutes-loading with H_2DCFDA). Thereafter, cells were exposed to DHA in the presence or absence of Tempol for 3

hours, followed by ROS measurement. (**C**) [^{3}H]thymidine incorporation in veh or DHA-treated hPASMC in the absence and presence of Tempol. (**D**) Representative Western blot of cyclin D1 protein expression in veh- or DHA-treated hPASMC in the presence and absence of Tempol. (**E**) Representative Western blot of phosphorylated eIF-2a in vehicle (veh) or DHA-treated hPASMC in the presence and absence of Tempol. Total eIF-2a served as loading control. Data are given as mean±SEM of at least 5 independent experiments. *P<0.05.

3.5. THE ROLE OF CA^{2+} AND MITOCHONDRIA IN DHA-INDUCED ROS GENERATION

To identify the underlying mechanisms responsible for ROS generation upon DHA treatment, we addressed whether or not Ca^{2+} signaling is involved in ROS generation. For this purpose cells were loaded with the intracellular Ca^{2+} chelator BAPTA-AM. Cells loaded with BAPTA-AM showed decreased ROS production in response to DHA (Fig. 12A). In order to examine the role of Ca^{2+} in DHA-induced ROS production in more detail, we first tested the capacity of DHA to modulate the cytosolic Ca^{2+} concentration ($[Ca^{2+}]_i$). DHA increased $[Ca^{2+}]_i$ in the absence and even more in the presence of extracellular Ca^{2+} (Fig. 12B). The importance of extracellular Ca^{2+} for DHA-induced ROS was demonstrated by decreased ROS in cells treated with DHA in the absence of extracellular Ca^{2+} (EGTA buffer) compared to cells in the presence of extracellular Ca^{2+} (Ca^{2+} buffer; Fig. 12C). These results showed that DHA-induced increase in intracellular Ca^{2+} is responsible and necessary for the increased ROS production in hPASMC. Furthermore, source of DHA-induced Ca^{2+} increase requires mobilization of both intracellular calcium stores and influx of extracellular calcium.

Events following increased intracellular Ca^{2+} were investigated further. Mitochondria are one of the major sites of intracellular ROS generation. Overall cellular DHA-induced ROS was decreased in the presence of RU360, a specific inhibitor of Ca^{2+} uptake into mitochondria (Fig. 12D). Also the DHA-induced

increase in mitochondrial ROS, measured in MitoSOX Red loaded cells, was markedly decreased by RU360 (Fig. 12E). Specificity of the MitoSOX signal was confirmed by co-localization studies using array scanning laser microscopy. The majority of MitoSOX Red accumulated in mitochondria as found by its co-localization with a mitochondria-specific marker MitoTracker Green (Fig. 13).

Although mitochondria are involved in the DHA-induced ROS production, the mitochondrial respiratory chain does not seem to be the source of the ROS production (Fig. 14). This is evidenced by the lack of effect of the mitochondrial respiratory chain inhibitors rotenone and TTFA, both of which were ineffective in suppressing DHA-induced ROS (Fig. 14).

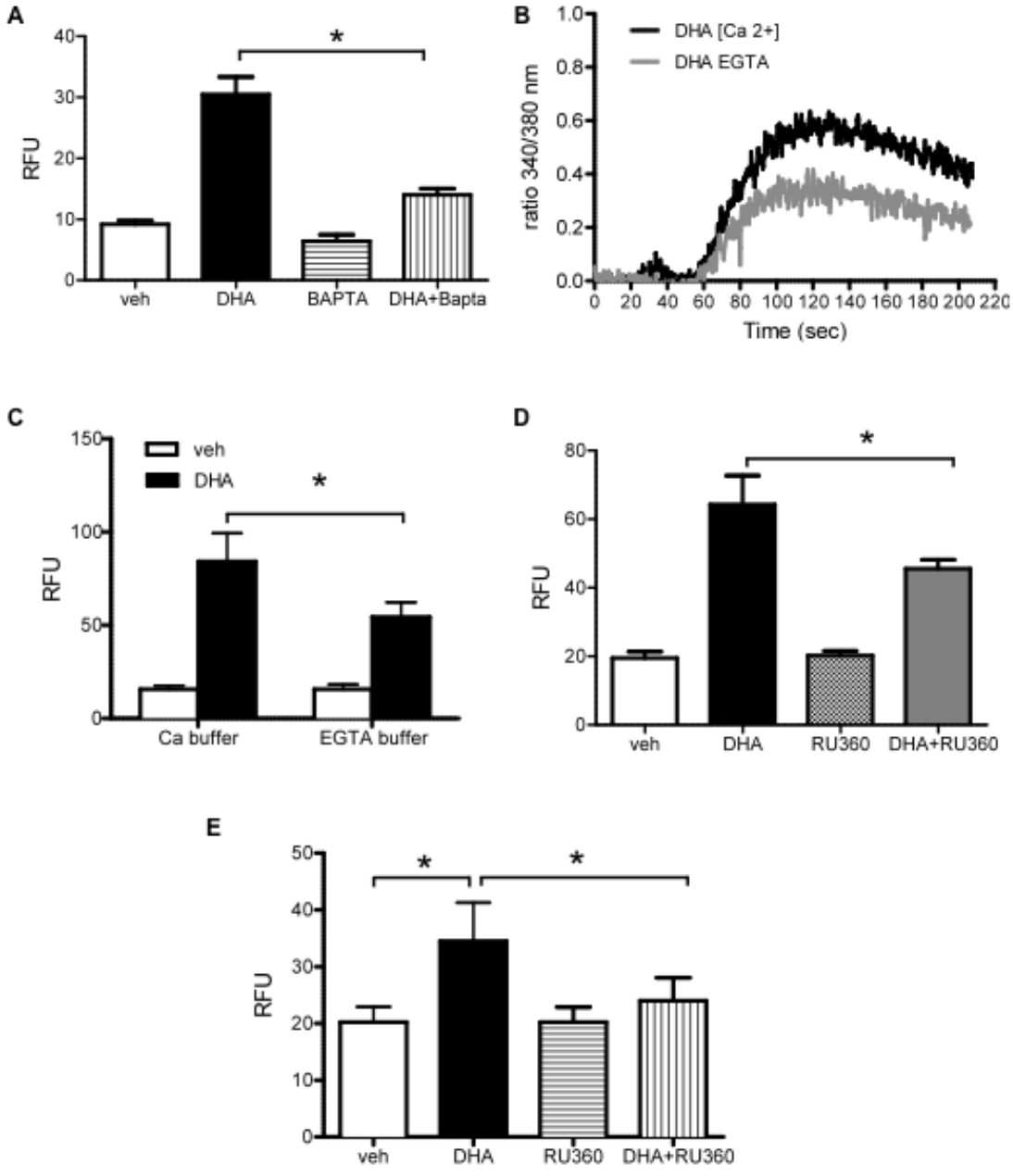

FIG. 12. Ca^{2+} and mitochondria are involved in DHA-induced ROS production. (**A**) hPASMC were loaded with H_2DCFDA (10 μM) in the presence or absence of Bapta-AM (5 μM) for 30 minutes. Then, cells were further incubated with vehicle or 100 μM DHA in the presence or absence of Bapta-AM for 1 hour, followed by ROS measurements by flow cytometry. (**B**) Fura-2/AM-loaded hPASMC were resuspended either in Ca^{2+} -containing buffer ([Ca^{2+}]) or Ca^{2+} -free

buffer containing EGTA (EGTA). The ratio of fura-2 fluorescence intensity at the two excitation wavelengths (340/380 ratio) was monitored fluorometrically in a stirring cuvette during exposure to vehicle (veh) or 10 µM DHA. Results are representative single traces out of three experiments performed in duplicate. Values for vehicle were subtracted from those obtained with DHA. Experiments were preformed by Monika Riederer. (**C**) Cells were loaded with H_2DCFDA in full medium with 5% FCS for 30 minutes. Then, cells were washed with calcium- or calcium free-buffer and incubated with vehicle or DHA in the respective buffers for 1 hour, followed by ROS measurements. Experiments were performed by Margarete Lechleitner. (**D**) Cells were loaded with H_2DCFDA in the absence or presence of RU360 for 30 minutes. Thereafter, cells were incubated with veh, RU360 (10 µM) or DHA±RU360 for 1 hour, followed by flow cytometric measurement of ROS. Experiments were performed by Margarete Lechleitner. (**E**) The procedure was exactly as described in (D) except cells were loaded with MitoSox Red (1 µM). Unless stated otherwise, data are given as mean±SEM of 6 independent experiments. *P<0.05.

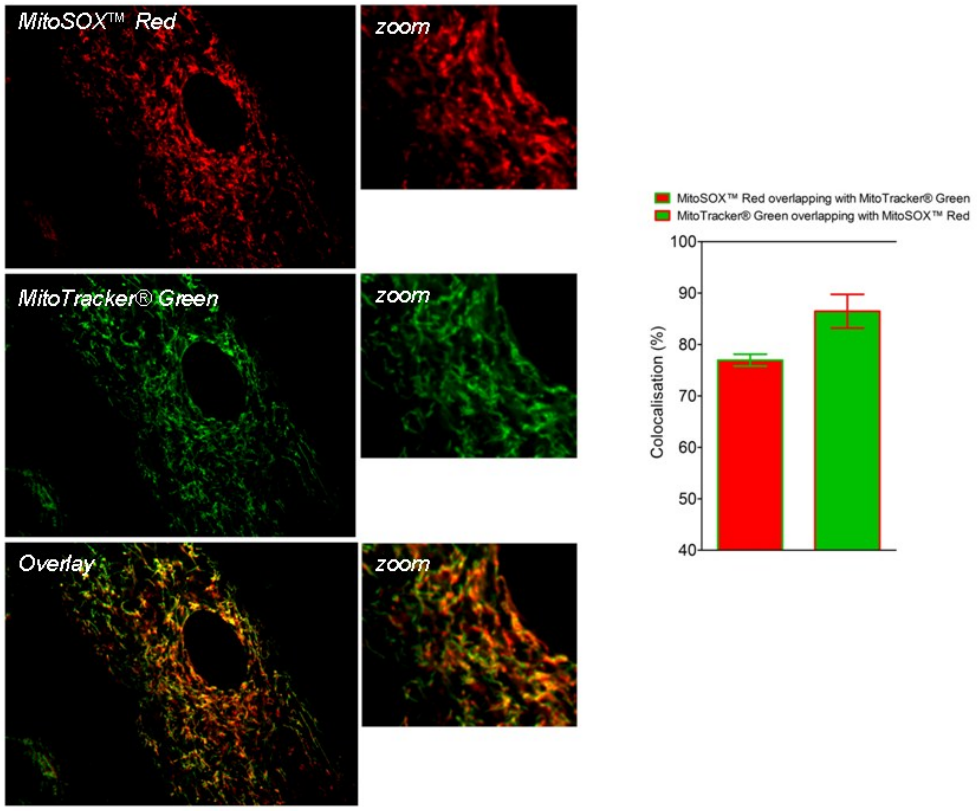

FIG. 13. MitoSox Red localizes to mitochondria of DHA treated cells. Cells loaded with MitoSox Red (1 μM) and MitoTracker Green (0.5 μM) for 30 minutes were further incubated with DHA for 60 minutes and analyzed by an array confocal laser scanning microscope. Image analysis (colocalization analysis) was performed using MetaMorph® Software 7.7 (n=8). Experiments were performed by Roland Malli.

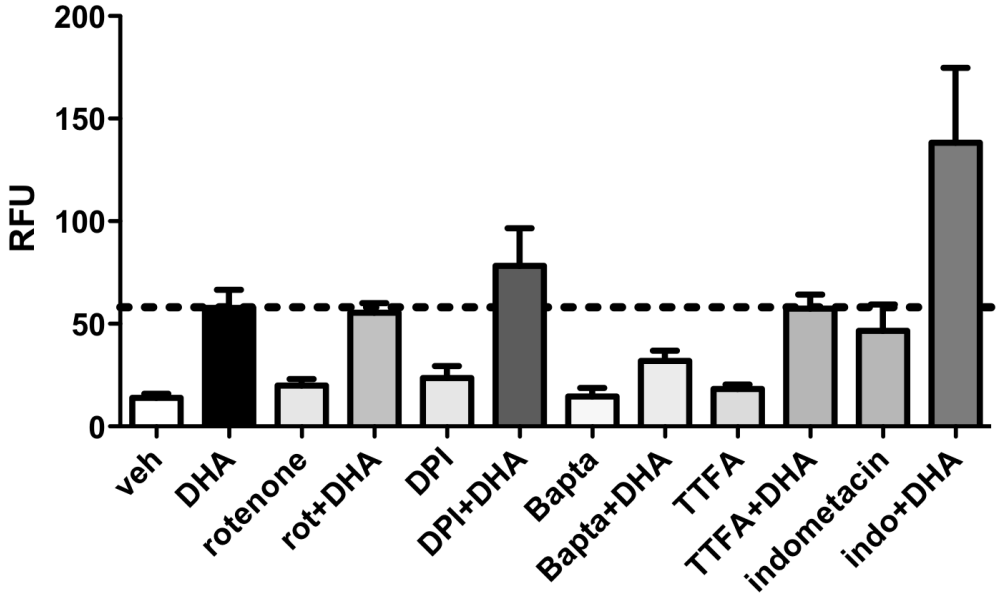

FIG. 14. Effect of mitochondrial respiratory chain inhibitors on DHA-induced ROS production in hPASMC. Cells were pre-incubated with inhibitors or veh (DMSO) for 2 h (90 min before loading and during 30 minutes-loading with H_2DCFDA). Thereafter, cells were exposed to DHA (100 μM) in the presence or absence of inhibitors for 1 h, followed by ROS measurement.

3.6. DHA INDUCES MITOCHONDRIAL MEMBRANE POTENTIAL ($\Delta\Psi$M) DISSIPATION, ATP DEPLETION AND APOPTOSIS IN HPASMC

Influx of calcium into mitochondria and subsequent ROS production indicated possible mitochondrial dysfunction and involvement of mitochondria in DHA-induced proliferation inhibition by induction of apoptosis. Indeed, both quantification of cleaved caspase-3 positive cells and TUNEL assay showed a significant induction of apoptosis upon prolonged DHA treatment (Fig. 15A, B). Importantly, Tempol markedly diminished DHA-induced apoptosis (Fig. 15C). Furthermore, DHA caused mitochondrial dysfunction as reflected by decreased $\Delta\Psi_m$ in DHA-treated cells (Fig. 15D). In line with the decreased $\Delta\Psi_m$, the cellular ATP content (Fig. 15E) and the ATP/ADP ratio (Fig. 15F) were decreased in DHA

treated cells, compared to respective control cells. Taken together, the results show that DHA-induced disturbances in intracellular calcium lead to increased ROS production in mitochondria with subsequent dissipation of mitochondrial membrane potential, decreased intracellular ATP levels and induction of apoptosis. Tempol experiments confirmed the central role of ROS in DHA-induced effects.

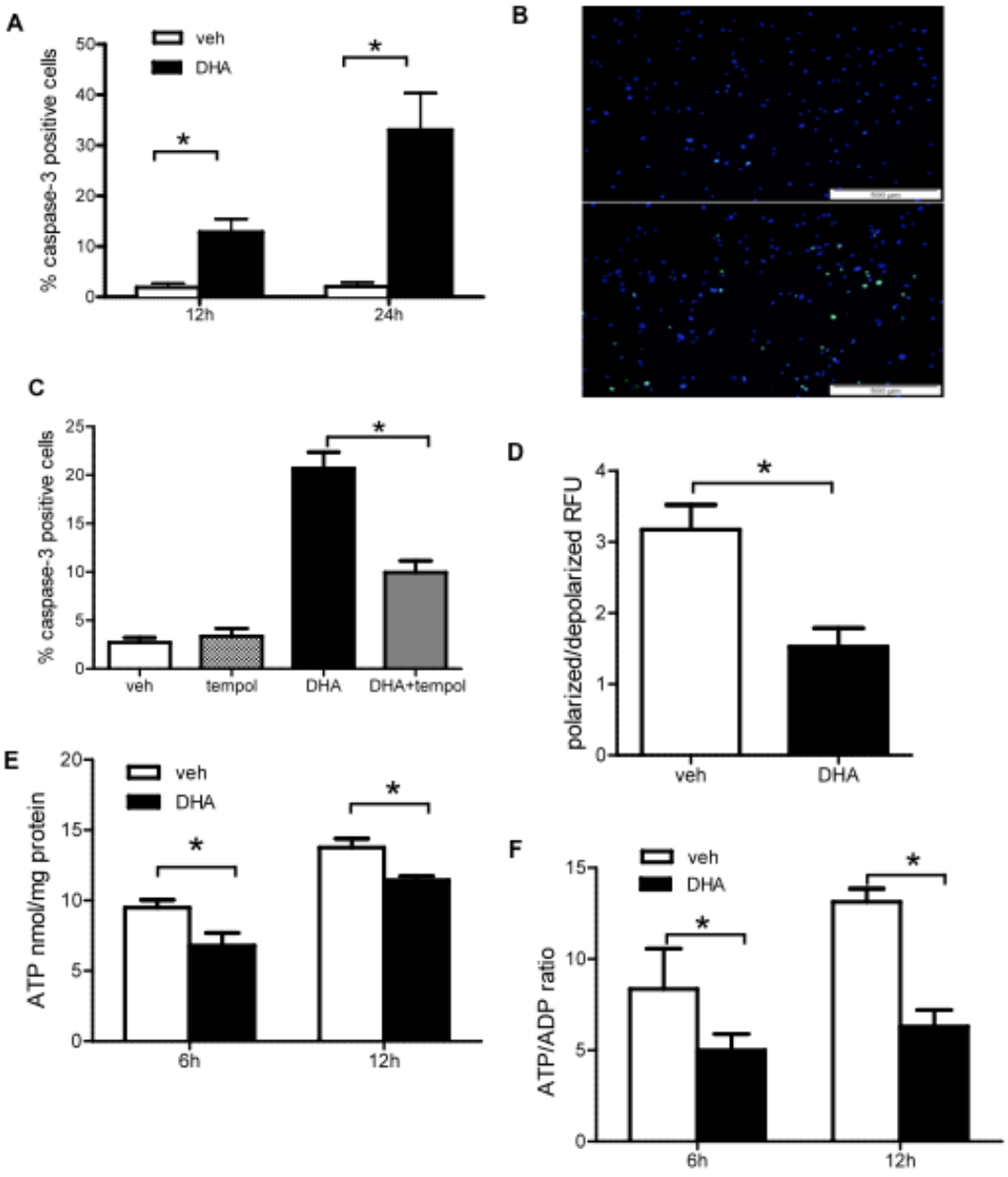

FIG. 15. DHA induces apoptosis in hPASMC. (**A**) Flow cytometric determination of cleaved caspase-3 positive cells. (**B**) Representative immunofluorescent staining for TUNEL positive cells (green) and DAPI counterstain. Upper panel shows veh treated and lower panel shows cells treated with DHA for 24 hours. (**C**) hPASMC were pre-incubated with Tempol or vehicle (veh) for 2 hours and treated

overnight with 100 µM DHA. Percentage of apoptotic cells was determined using flow cytometric assay for cleaved caspase-3. (**D**) Flow cytometric determination is presented as decreased orange/green ratio indicative of a reduced MMP, as described in Methods. Data are given as mean±SEM of 6 independent experiments. *P<0.05 vs corresponding vehicle control group. (**E**) Cellular ATP content after 6 h and 12 h incubation with vehicle or 100 µM DHA. Experiments were performed by Seth Hallström. (**F**) Cellular ATP/ADP ratio after 6 hours and 12 hours incubation with vehicle or 100 µM DHA. Experiments were performed by Seth Hallström. Results are mean±SEM of 6 separate incubations for veh and DHA for each indicated time point. *P<0.05

Although DHA-induced mitochondrial influx of calcium has an initiating role in ROS production and later on mitochondrial dysfunction, RU360 was not sufficient to block DHA anti-proliferative effects on hPASMC (Fig. 16).

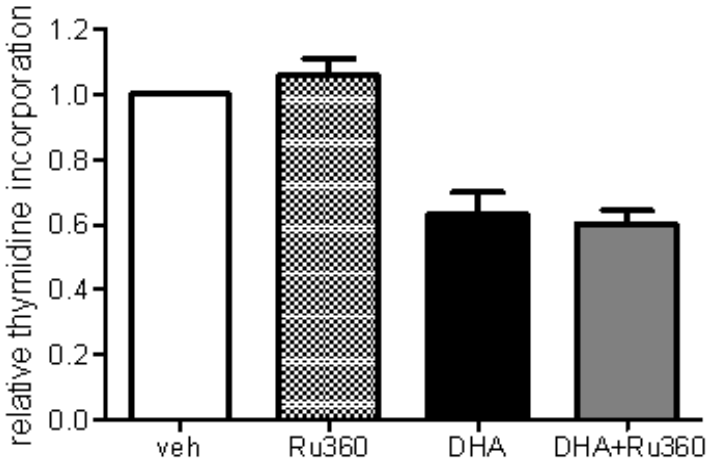

FIG. 16. RU360 fails to counteract DHA-mediated attenuation of cell proliferation. Cells were plated in 96-well plates and incubated without or with RU360 (10 µM) for 1 hour before further incubation with vehicle or DHA (100 µM) along with 2 µCi/well [methyl-3H]thymidine in the absence or presence of RU360

for 24 h. Thereafter, cells were harvested and radioactivity measured in a scintillation counter. Data are mean±SEM of 4 independent experiments. *P<0.05.

3.7. EFFECT OF OMEGA-3 PUFA-RICH DIET ON THE DEVELOPMENT OF EXPERIMENTAL PULMONARY HYPERTENSION

Hypoxia-induced pulmonary hypertension in mice is an established animal model to study pulmonary vascular remodeling, characterized by appearance of smooth muscle cell layer around normally non-muscularized pulmonary vessels. Based on the obtained in vitro data, which showed inhibited proliferation of pulmonary vascular smooth muscle cells by members of omega-3 PUFA, we speculated that animals fed with omega-3 PUFA rich diet (diet containing fish oil) and exposed to hypoxia, would be protected against the development of pulmonary vascular remodeling and pulmonary hypertension compared to animals fed with isocaloric diet (corn oil diet).

The possible beneficial role of fish oil rich diet was tested in a preventive experimental setup. Adult male mice were fed 2 weeks prior to normoxia/hypoxia exposure with fish oil diet, corn oil diet (isocaloric control diet) and chow diet and further 5 weeks during normoxia/hypoxia exposure.

Corn oil fed mice exhibited a trend of higher total body weight in both normoxic and hypoxic animals (Fig. 17). Hypoxic animals lost weight (data not shown) at the beginning of the hypoxia exposure, however, weight loss stabilized and eventually animals began gaining weight again, although they did not reach the level of normoxia-exposed animals (Fig. 17).

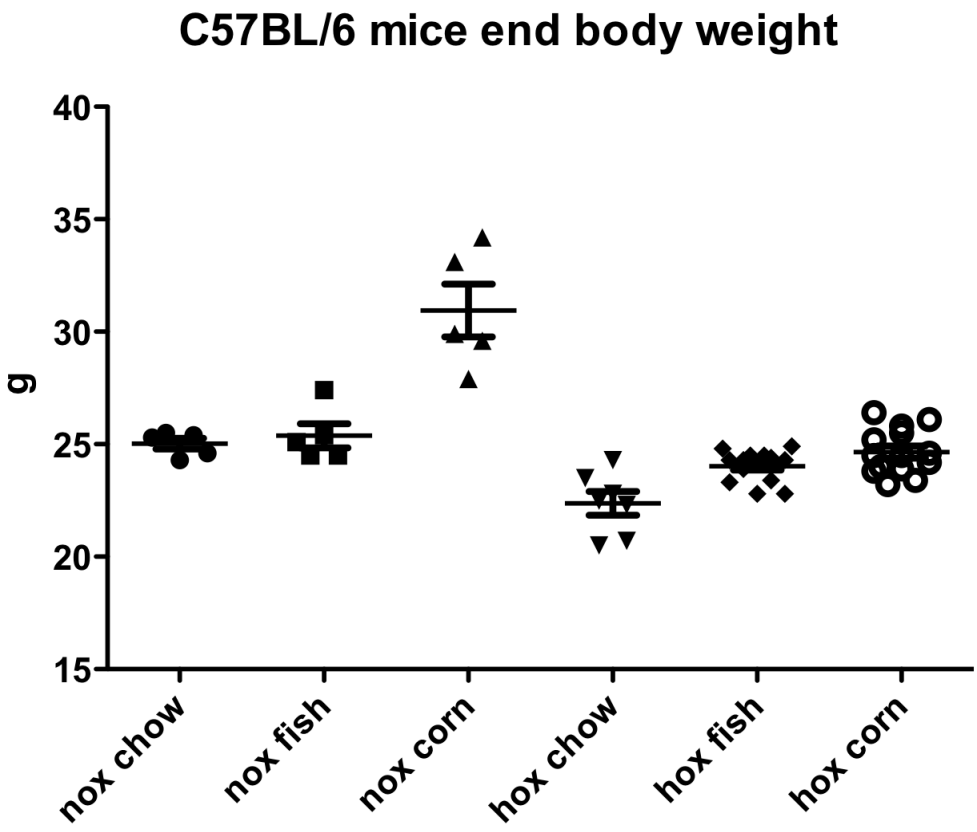

FIG. 17. Effect of hypoxia and diet on total body weight. Fifty C57Bl mice were fed with chow, fish oil or corn oil diet for 7 weeks and exposed to 10% normobaric hypoxia for 5 weeks. Total body weight was determined at the end of the experiment. Data points represent individual animals, horizontal lines mean values and bar SEM.

Animals fed with fish and corn oil diet showed also a trend of increased liver wet weight, both in normoxia and hypoxia (Fig. 18). However, there was no increase in liver wet weight hypoxia-exposed animals (Fig. 18).

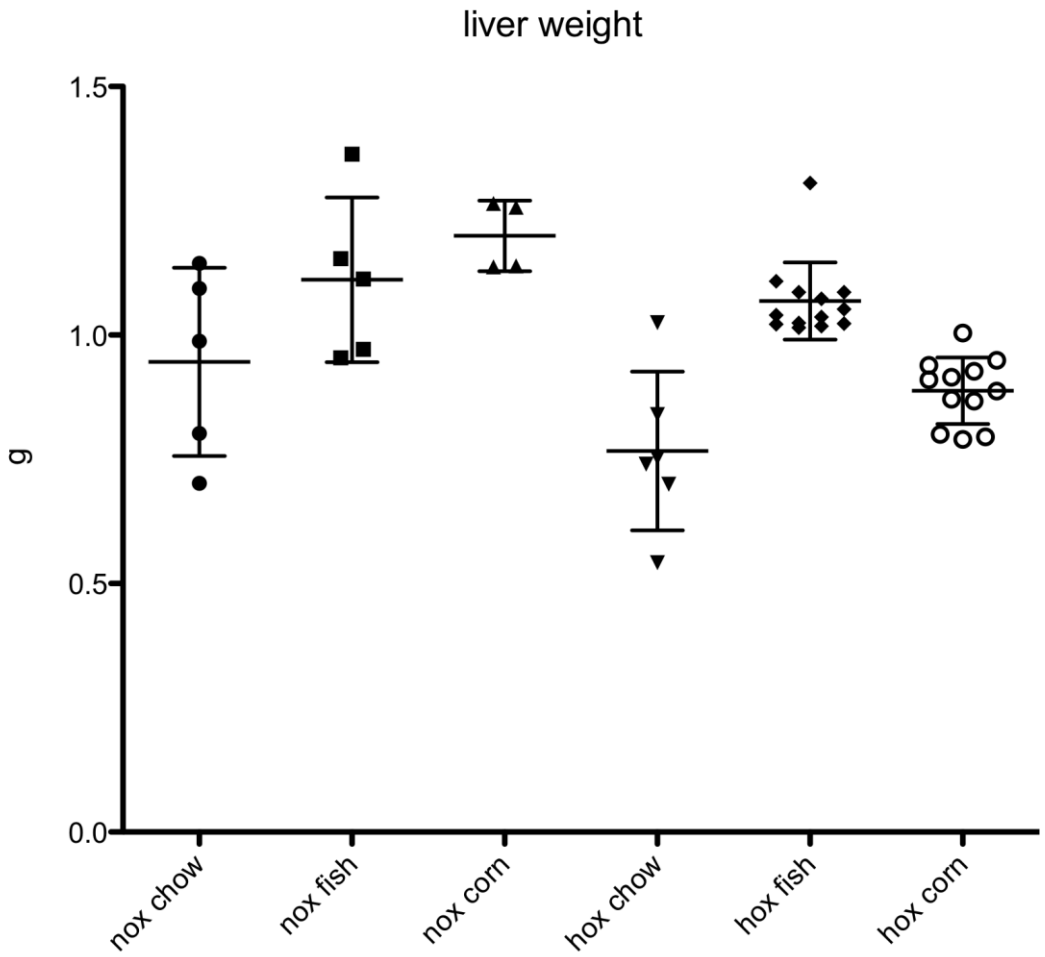

FIG. 18. Effect of hypoxia and diet on liver wet weight. Fifty C57Bl mice were fed with chow, fish oil or corn oil diet for 7 weeks and exposed to 10% normobaric hypoxia for 5 weeks. Animals were sacrificed at the end of the hypoxia exposure and the liver wet weight was determined. Data points represent individual animals, horizontal lines mean values and bar SEM.

Lung lipid content of various fatty acids that belong to omega-3 PUFA was significantly increased in fish oil fed animals (Fig. 19). Concomitantly, lung content of omega-6 PUFA was significantly decreased in fish oil fed animals (Fig. 19). These results show that the feeding regiment was efficient in enriching the lungs with omega-3 PUFA and depleting them with omega-6 PUFA.

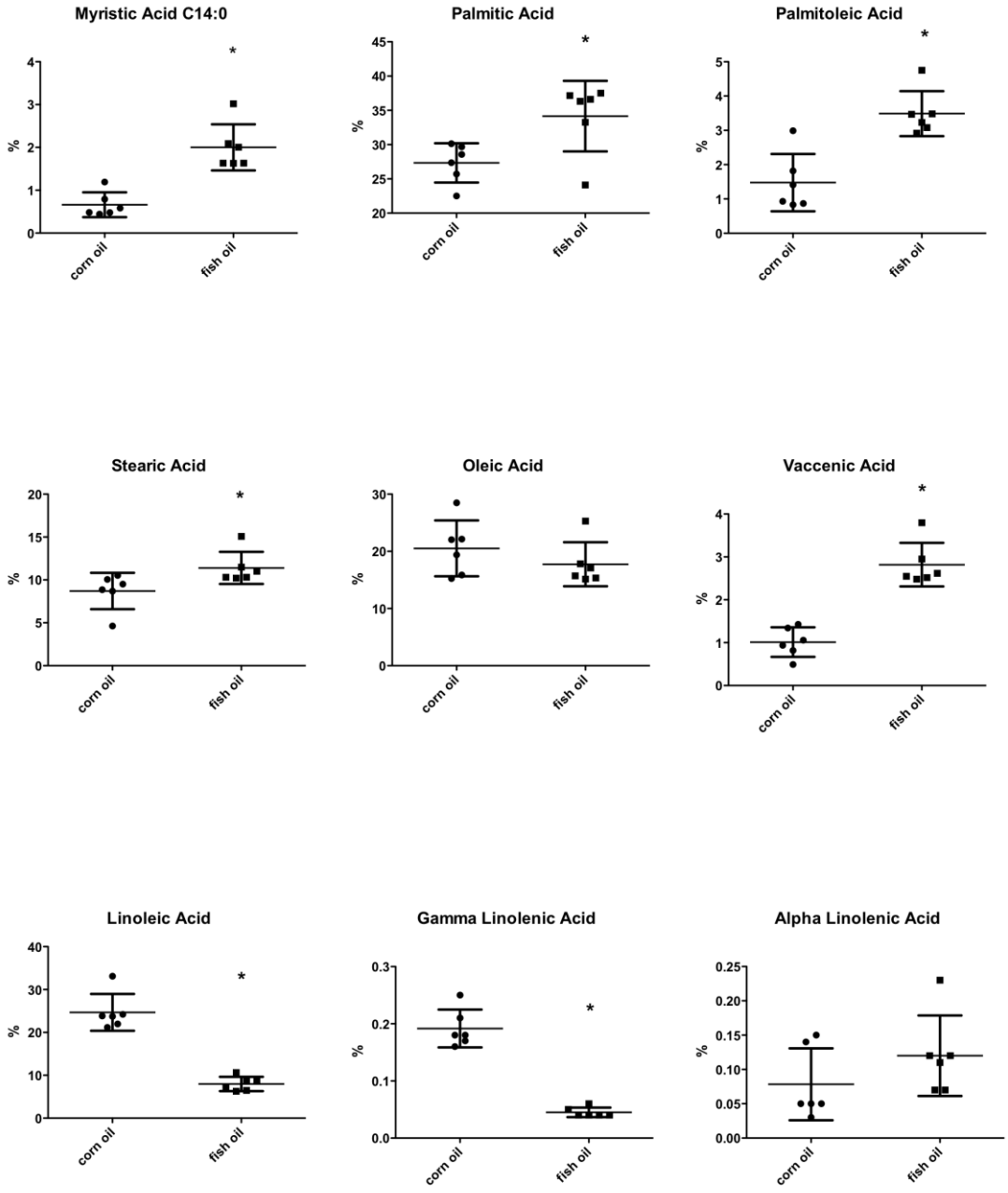

FIG. 19. Effect of diet on fatty acid composition in the lungs. Fifty C57Bl mice were fed with chow, fish oil or corn oil diet for 7 weeks. Fatty acid composition in the lungs was determined by mass spectrometry. Mass spectrometric analysis was performed by ZMF Mass Spectrometry Core Facility. Data points represent individual animals, horizontal lines mean values and bar SEM. *P<0.05 by t-test.

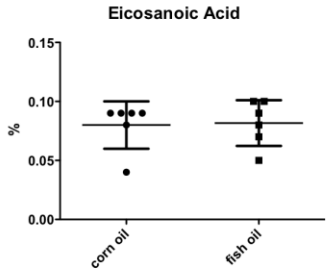
Eicosanoic Acid
%
0.15
0.10
0.05
0.00
corn oil
fish oil

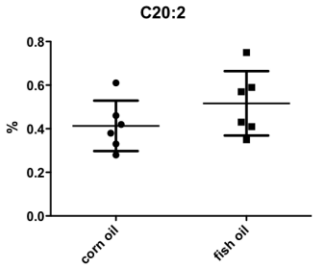
C20:2
%
0.8
0.6
0.4
0.2
0.0
corn oil
fish oil

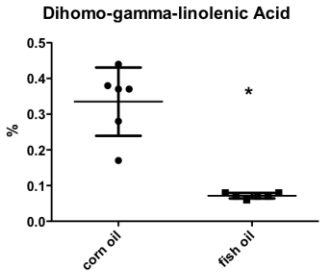
Dihomo-gamma-linolenic Acid
%
0.5
0.4
0.3
0.2
0.1
0.0
*
corn oil
fish oil

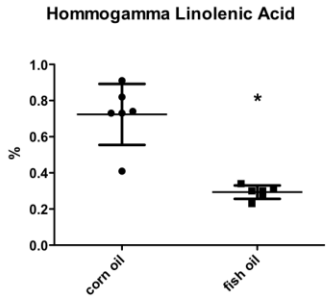
Hommogamma Linolenic Acid
%
1.0
0.8
0.6
0.4
0.2
0.0
*
corn oil
fish oil

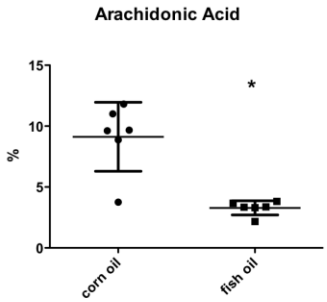
Arachidonic Acid
%
15
10
5
0
*
corn oil
fish oil

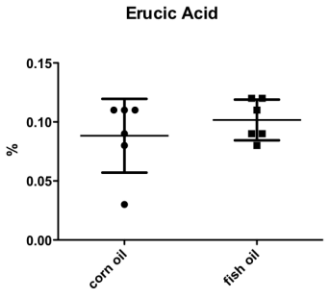
Erucic Acid
%
0.15
0.10
0.05
0.00
corn oil
fish oil

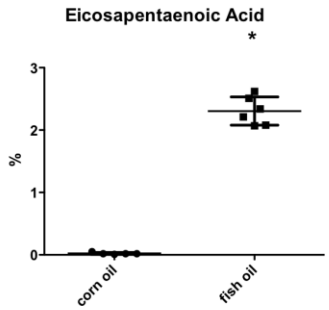
Eicosapentaenoic Acid
%
3
2
1
0
*
corn oil
fish oil

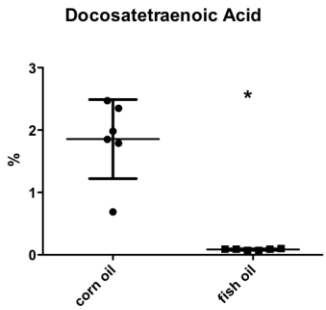
Docosatetraenoic Acid
%
3
2
1
0
*
corn oil
fish oil

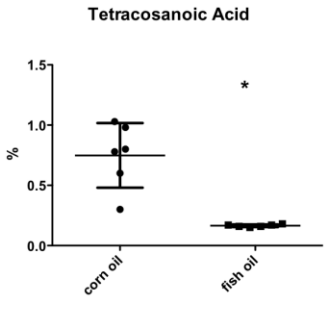
Tetracosanoic Acid
%
1.5
1.0
0.5
0.0
*
corn oil
fish oil

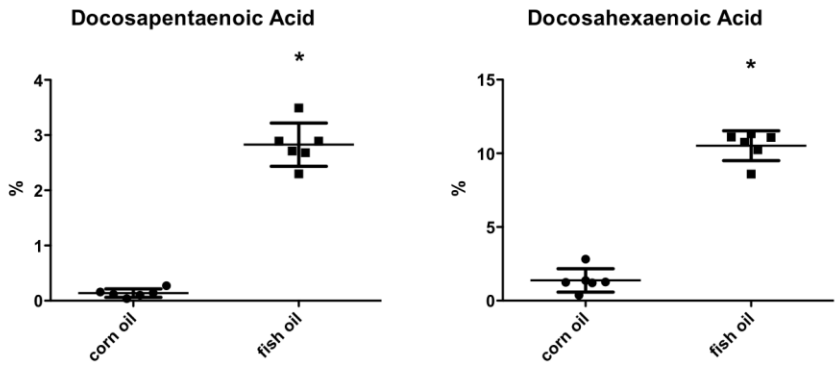

FIG. 19. Effect of diet on fatty acid composition in the lungs (continued).

The influence of fish oil diet on the development of hypoxia-induced pulmonary hypertension in mice was indirectly assessed by measuring right ventricle hypertrophy expressed as Fulton index (wet weight ratio of right ventricle to left ventricle and septum). Five weeks exposure to hypoxia led to a significant increase of Fulton index in the case of all feeding regiments (Fig. 20), indicating that all hypoxic animals developed right ventricle hypertrophy. However, there was a difference in right ventricle hypertrophy between chow, fish or corn oil fed animals under hypoxia (Fig. 20).

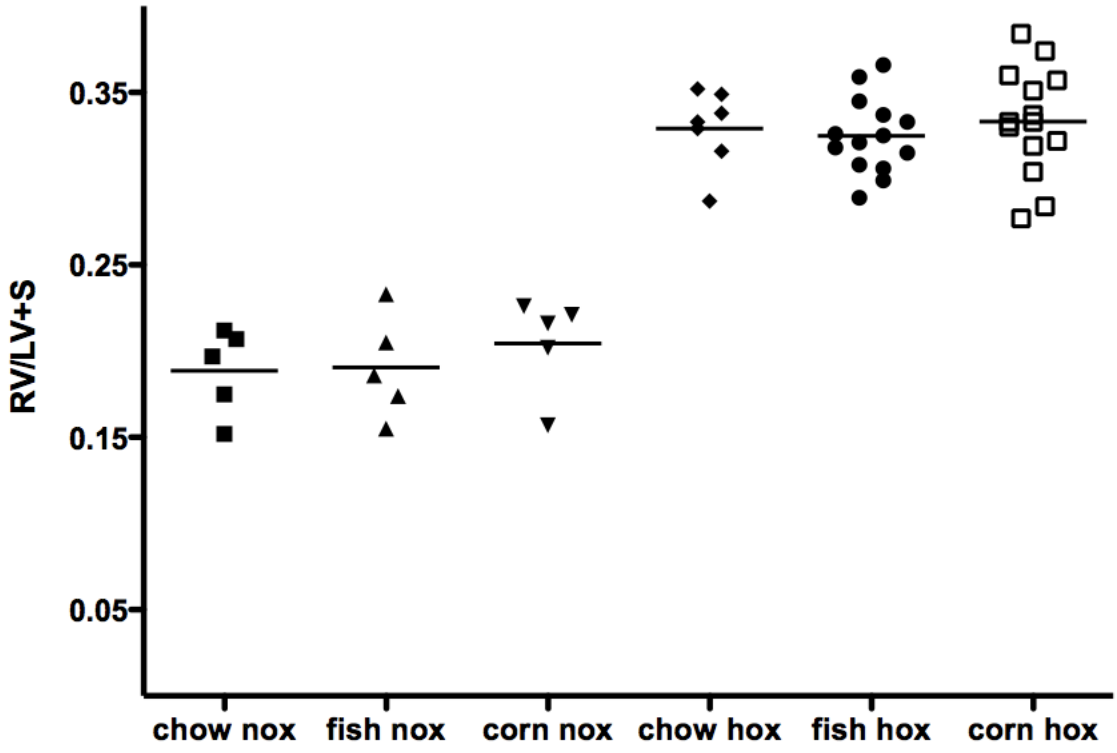

FIG. 20. Effect of hypoxia and diet on right ventricular hypertrophy (Fulton index). Fifty C57Bl mice were fed with chow, fish oil or corn oil diet for 7 weeks and exposed to 10% normobaric hypoxia for 5 weeks. Animals were sacrificed at the end of the hypoxia exposure; the right ventricle was dissected from rest of the heart (left ventricle and septum) and wet weight was determined for both right ventricle and left ventricle plus septum. Data points represent individual animals and horizontal lines mean values.

The second main characteristic of pulmonary hypertension is pulmonary vascular remodeling. We determined the level of pulmonary vascular remodeling in chow fed mice held under normoxia and hypoxia. Remodeling was evaluated as percentage wall thickness of pulmonary arteries from hematoxilin-eosin stained lung slices (Fig. 21). Percentage wall thickness was calculated by measuring the vessel wall thickness and dividing it by the external diameter.

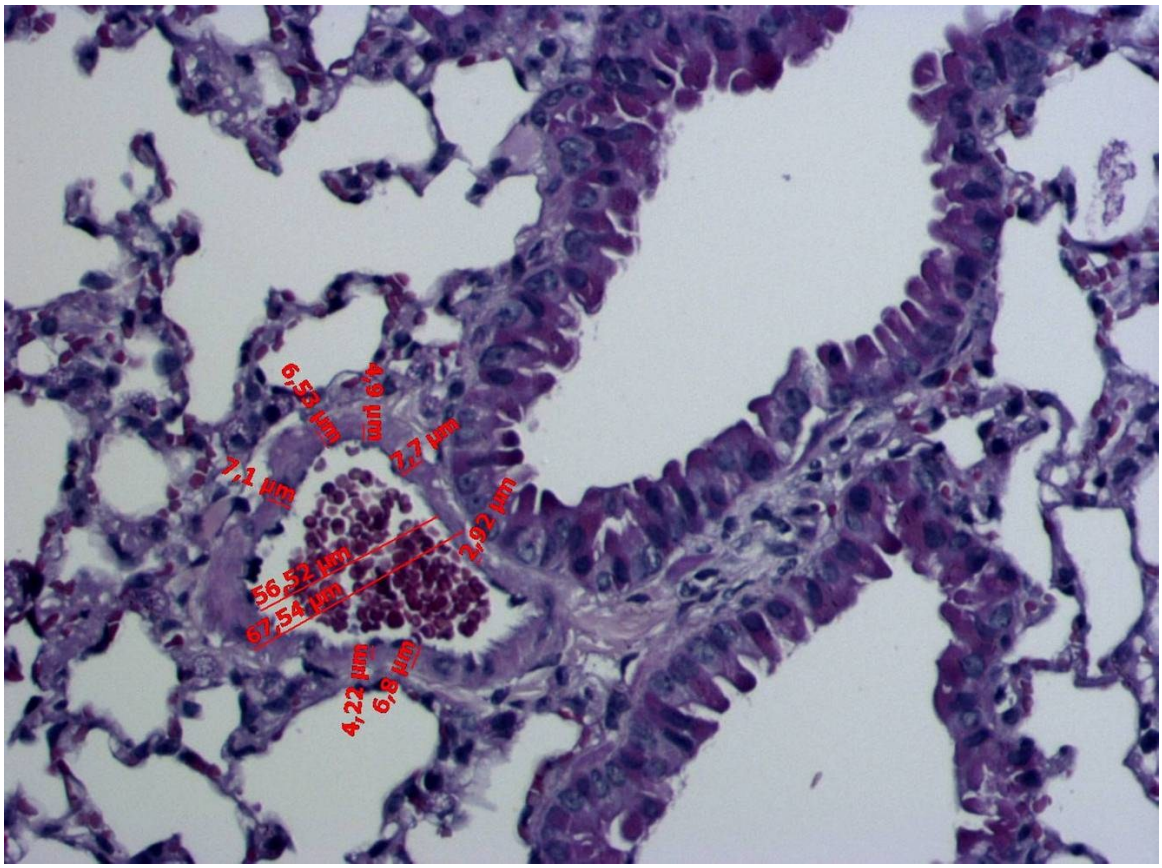

FIG. 21. Representative photomicrograph of a mouse pulmonary artery and the percentage vessel wall thickness measurement. C57Bl mice were fed with chow, fish oil or corn oil diet for 7 weeks and exposed to 10% normobaric hypoxia for 5 weeks. Animals were sacrificed at the end of the hypoxia exposure; the left lung lobe dissected, fixed overnight in 4% formalin and embedded in paraffin. Two micrometer thick paraffin slices were rehydrated and stained with hematoxilin-eosin staining. Percentage vessel wall thickness measurements were performed by Snjezana Cuzic.

Although percentage wall thickness did show a trend increase in hypoxic animals, particularly on the level of the small alveolar duct associated pulmonary vessels, this method for pulmonary vascular remodeling analysis proved to be time consuming, low sensitivity and prone to errors. Therefore, due to the lack of an effect on the right ventricle hypertrophy, the effect of fish oil diet on pulmonary vascular remodeling was not assessed further.

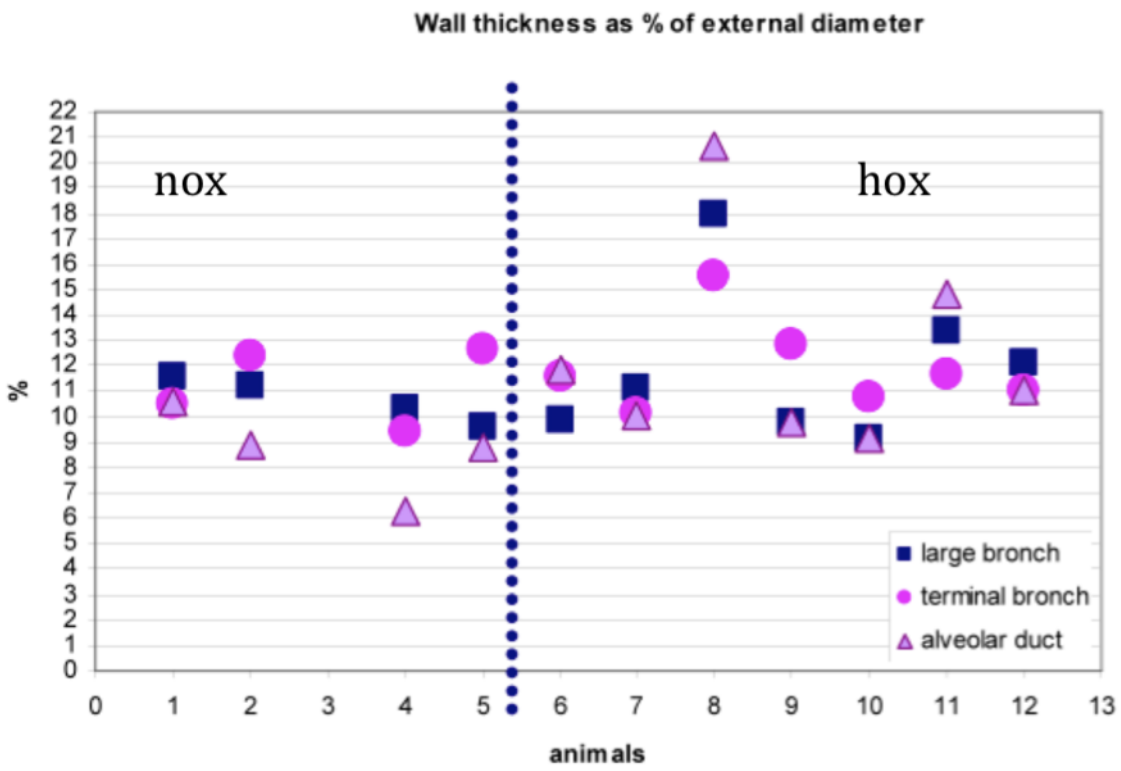

FIG. 22. Percentage vessel wall thickness measurement. C57Bl mice were fed with chow, fish oil or corn oil diet for 7 weeks and exposed to 10% normobaric hypoxia for 5 weeks. Animals were sacrificed at the end of the hypoxia exposure; the left lung lobe dissected, fixed overnight in 4% formalin and embedded in paraffin. Two micrometer thick paraffin slices were rehydrated and stained with hematoxilin-eosin staining. Percentage vessel wall thickness measurements were performed by Snjezana Cuzic.

Even though fish oil diet regiment efficiently enriched lung lipids with omega-3 fatty acids, including DHA, due to the lack of effect on right ventricular hypertrophy, we investigated the possibility that the lack of observed effect might be due to inefficient induction of oxidative and ER stress response in the lungs. Gene expression analysis of ER and oxidative stress marker genes indeed revealed a

weak increase in the ER stress marker HSPA5 and in the oxidative stress marker HO-1 (HMOX1) in fish oil versus chow diet fed animals (Fig. 23). Hypoxia responsive gene EroL-1α also show a slight increase in hypoxic animals (Fig. 23). However, ER stress marker EroL-1β showed no change in fish oil versus chow diet fed animals (Fig. 23).

Free fatty acids, including omega-3 PUFA, present in fish oil diet, exert some of their effects through induction of PPAR family of transcription factors. Gene expression analysis confirmed the presence of both PPARδ and PPARγ in mouse lung tissue (Fig. 23). In addition, hypoxic animals showed a trend of increased PPARδ expression (Fig. 23).

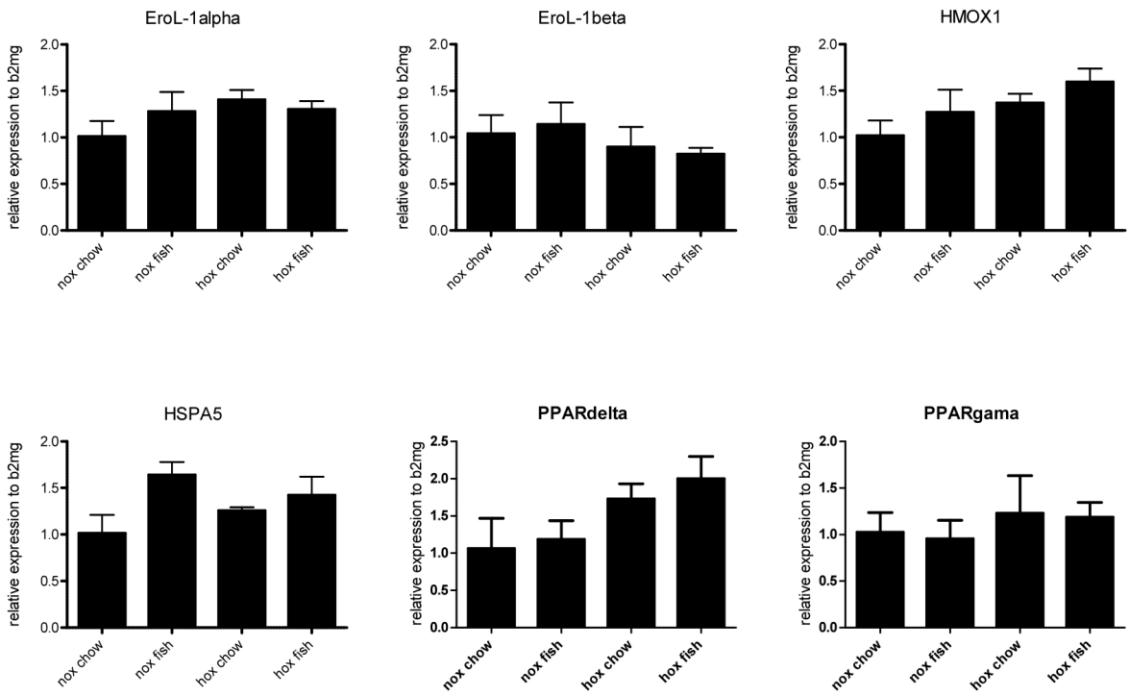

FIG. 23. Gene expression changes in oxidative and ER stress marker genes and fatty acid activated transcription factor genes in mice lungs. Fifty C57Bl mice were fed with chow, fish oil or corn oil diet for 7 weeks and exposed to 10% normobaric hypoxia for 5 weeks. Relative gene expression of ER stress markers

(EroL-1β, HSPA5), oxidative stress (HMOX1, EroL-1α) and fatty acid activated transcription factors (PPARdelta, PPARgamma) was determined by quantitative RT-PCR from lung homogenates. Data were normalized using beta-2 microglobulin as housekeeping gene. Data are given as mean±SEM from 4 animals in each group.

Despite the presence of both transcription factors responsive to free fatty acids, gene expression analysis of PPARα (Aldh3a2, Cpt1a, Pdk4), PPARδ (ApoE, CD36) and PPARγ (Anglpt4, Fabp5, Pln2) responsive genes showed no indication of PPAR downstream signaling pathway activation (Fig. 24).

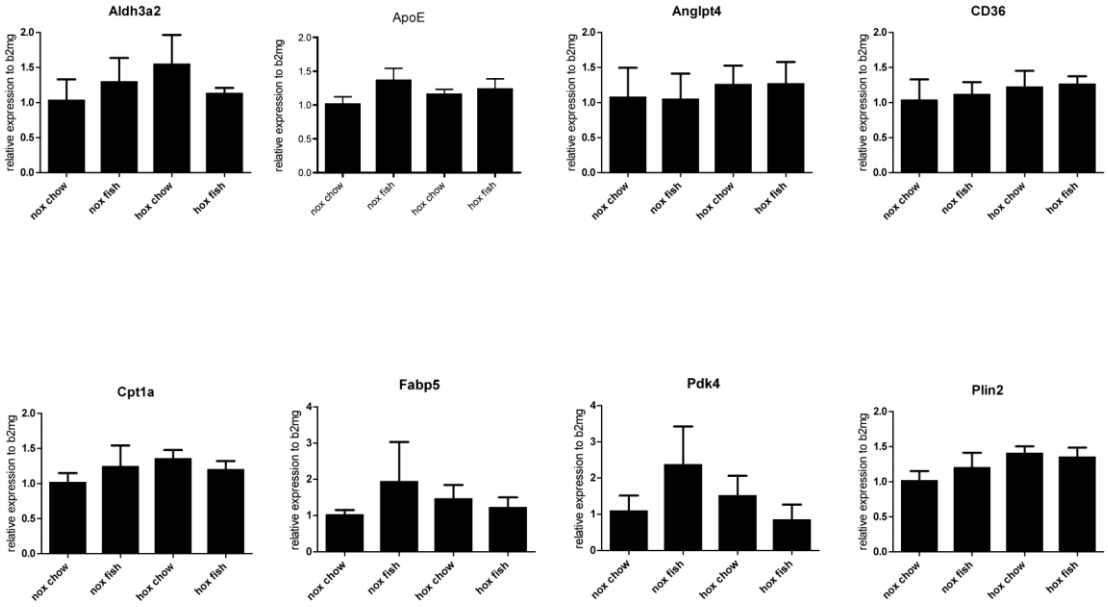

FIG. 24. Gene expression changes in PPAR responsive genes in the mouse lungs. Fifty C57Bl mice were fed with chow, fish oil or corn oil diet for 7 weeks and exposed to 10% normobaric hypoxia for 5 weeks. Relative gene expression of PPARα (Aldh3a2, Cpt1a, Pdk4), PPARγ (ApoE, CD36) and PPARδ (Anglpt4, Fabp5, Pln2) responsive genes was determined by quantitative RT-PCR from lung

homogenates. Data were normalized using beta-2 microglobulin as housekeeping gene. Data are given as mean±SEM from 4 animals in each group.

In order to clarify a potential increase in oxidative and ER stress marker genes, a more detailed gene expression experiment was performed on hypoxia-exposed mice of all 3 diet regiments.

The oxidative stress marker gene HO-1 showed a slight but significant increase only in corn oil fed mice (Fig. 25).

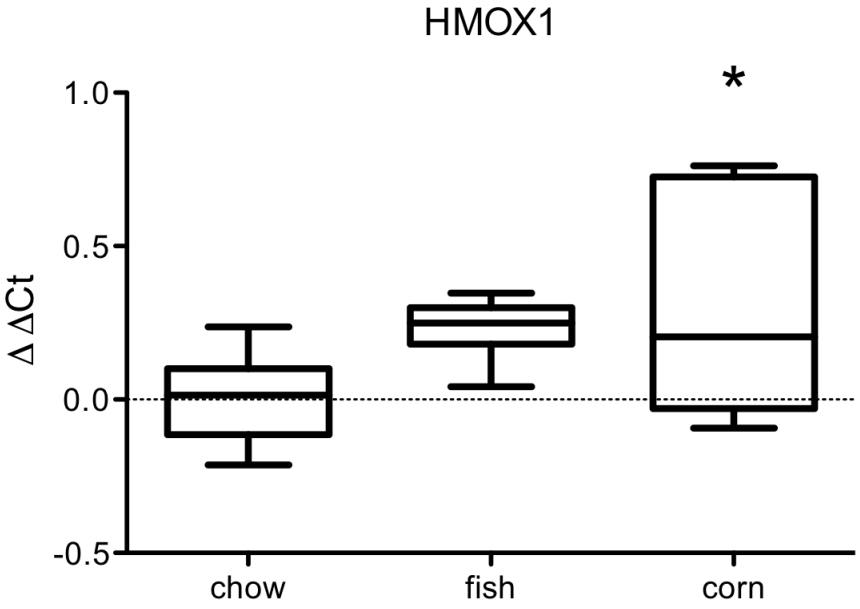

FIG. 25. Gene expression changes in heme oxygenase 1 (HMOX1) in hypoxic mice fed different diets. C57Bl mice were fed with chow, fish oil or corn oil diet for 7 weeks and exposed to 10% normobaric hypoxia for 5 weeks. The relative gene expression of the oxidative stress marker HMOX1 was determined by quantitative RT-PCR from lung homogenates. Data was normalized using beta-2 microglobulin as housekeeping gene. Data were given as mean±SEM from 7

animals in each group. *P<0.05 by ANOVA Kruskal-Wallis with the Dunn's multiple comparison post-test.

Finally, although ER stress marker gene HSPA5 was increased in fish oil fed mice, it was also significantly increased in corn oil fed animals (Fig. 26).

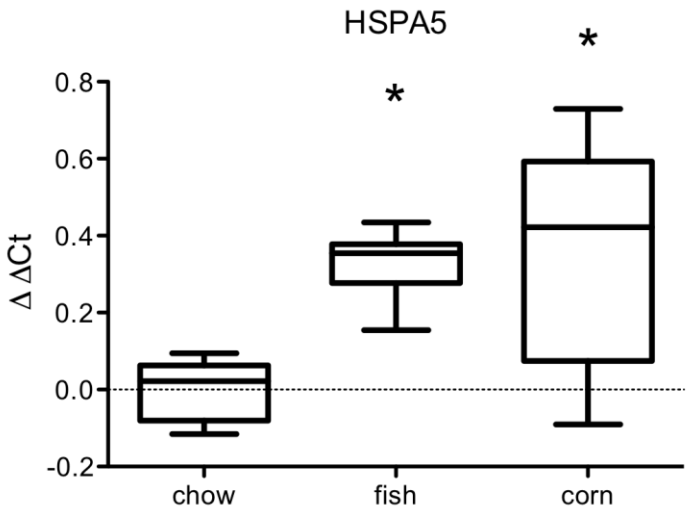

FIG. 26. Gene expression changes in HSPA5 in hypoxic mice fed different diets. C57Bl mice were fed with chow, fish oil or corn oil diet for 7 weeks and exposed to 10% normobaric hypoxia for 5 weeks. The relative gene expression of the ER stress marker HSPA5 was determined by quantitative RT-PCR from lung homogenates. Data were normalized using beta-2 microglobulin as housekeeping gene. Data are given as mean±SEM from 7 animals in each group. *P<0.05 by ANOVA Kruskal-Wallis with the Dunn's multiple comparison post-test.

4. DISCUSSION

The major finding of the present study is that DHA-induced oxidative stress is the initial and central event responsible for the induction of UPR, the inhibition of cell proliferation and the induction of apoptosis in hPASMC.

These effects of DHA were observed in fully supplemented medium containing serum and growth factors, thus closely resembling the *in vivo* conditions. There the cells are exposed to both circulating growth factors and ones that are attached to extracellular matrix proteins surrounding hPASMC or secreted by neighboring cells. Since DHA as a potential therapy for pulmonary vascular remodeling would be taken orally, it would be transported to the site of action – pulmonary vasculature, by blood. DHA as a highly lipophilic molecule exhibits strong binding to plasma proteins, including albumin. It was therefore decided to use medium containing 5% fetal bovine serum to closely resemble the in vivo pharamacokinetic profile.

4.1. DHA POTENTLY INHIBITS THE PROLIFERATION OF HPASMC UNDER DIFFERENT CONDITIONS

The effect of DHA on hPASMC proliferation was assessed by direct cell counting and by the thymidine incorporation method. Cell counting method gives the most reliable and direct assessment of compound's effect on cell proliferation. However, it is a time-consuming method and, as an end-point method, cannot differentiate between the relative contribution of diminished proliferation versus increased apoptosis or necrosis. Radioactively labeled thymidine incorporation assay was used as a second hPASMC proliferation readout. Although usage of triciated thymidine is required, it is a sensitive method to assess cell proliferation. However, it is only an indirect measurement of cell proliferation. Thymidine is incorporated during S phase of cell cycle into cellular DNA. Since it has to be phosphorylated by

thymidine kinase, incorporation rate can also depend on the activity of the thymidine kinase.

In accordance with the described anti-proliferative effect of DHA (38), the proliferation rate of hPASMC was markedly decreased by DHA (Fig. 1). Importantly, the applied concentrations of DHA, exhibiting an anti-proliferative effect in hPASMC, were within physiologically/ pharmacologically reachable levels in the human serum (39-43). In addition, cells were exposed to either normoxia or hypoxia. Hypoxia is a known factor causing pulmonary vascular remodeling. DHA showed a similar effect on hPASMC proliferation in both normoxia and hypoxia, although the overall proliferation was lower in hypoxia. Although hypoxia is described in the literature as a proliferative stimulus for hPASMC (44), decreased proliferation of hPASMC under hypoxia (Fig. 2) is in accordance to a report published by Morrell et al. (45,46). The exact reason for this discrepancy is unknown but it could be due to different origin of the primary hPASMC used. Another possible reason could be the use of different levels of hypoxia and different instruments to achieve hypoxic environment. System at our disposal assures a constant and reliable monitoring and maintaining of hypoxic conditions, therefore preventing occasional reoxygenation episodes due to opening and closing of culture chambers.

DHA also effectively inhibited PDGF-induced hPASMC proliferation (Fig. 3). This is of potential clinical significance since drugs targeting the PDGF growth factor signaling pathway have been shown to reverse pulmonary vascular remodeling and improve experimental pulmonary hypertension (15).

4.2. DHA SHOWS THE MOST POTENT EFFECT AMONG ALL TESTED PUFA

As a part of an approved pharmacological therapy for hypertriglyceridemia, another omega-3 fatty acid is also present in even higher concentrations, namely EPA. EPA also dose-dependently inhibited hPASMC proliferation determined by

cell counting (Fig. 4) although this effect was lower in comparison to DHA. DHA is described as having the most pronounced effects among omega-3 fatty acids. It is speculated that this is due to its high number of reactive unsaturated double bonds in its structure (47). Similarly, α-linolenic acid showed a very weak efficiency in inhibiting hPASMC, proliferation when compared to DHA (Fig 5). However, arachidonic acid (a member of omega-6 fatty acids) that also has a high number of reactive, unsaturated bonds like DHA, showed a significantly lower potency in inhibiting hPASMC proliferation (Fig. 5). Despite this, it implies that the inhibitory effect on hPASMC proliferation is not unique to omega-3 fatty acids but that it can also include other members of PUFA, including omega-6 fatty acids.

4.3. DHA-INDUCED G1 CELL CYCLE BLOCK IN HPASMC

A potential mechanism leading to decreased cell proliferation is block in cell cycle transition (48). A number of anti-neoplastic agents exert their action by causing an irreparable DNA damage that signals to cell cycle progression check points and blocks the cell division and progression into the next phase of cell cycle (48). The DHA effect on the cell cycle progression was investigated by flow cytometric determination of the DNA content (Fig. 6). Decreased hPASMC proliferation under DHA treatment was accompanied by an increased number of cells in the G1 phase of the cell cycle, a hallmark of G1 cell cycle block. This proved that DHA is able to a cause cell cycle progression block in hPASMC and thereby affect the proliferation of hPASMC.

On a molecular level, DHA decreased cyclin D1 protein content in hPASMC as measured by Western blot (Fig. 6). An increase in cyclin D1 protein content promotes and is necessary for the progression through G1 phase (49), further supporting the G1 cell cycle block finding. On the other hand, an increase in p21 protein content is associated with a block in cell cycle progression (50). Although DHA did not show an increase in p21 protein content measured by Western blot (Fig. 6), it is possible that some other negative regulator of cell cycle progression,

like p27, is increased under DHA treatment (51). Interestingly, DHA caused a decreased gene expression of p21 in hPASMC but not p27 (data not shown). However, this was not investigated further.

4.4. DHA-INDUCED UPR IN HPASMC

Reports showed that the unfolded protein response (UPR) can lead to cell cycle arrest (52) and that DHA is able to cause UPR. DHA was found to induce ER stress and UPR in colon cancer cells (53). However, a recent publication showed no evidence of ER stress and UPR in DHA-treated rat hepatocytes (54), indicating species and cell type specific cellular responses to DHA. UPR is characterized by an activation of ER membrane residing sensors: chaperon protein Bip (HSPA5), ER transmembrane kinase protein kinase RNA-like endoplasmic reticulum kinase (PERK) and ER transmembrane nuclease IRE1. Dissociation of Bip, and its binding to unfolded proteins accumulating in ER lumen, from PERK and IRE1 leads to downstream signaling cascades. Activation of the PERK cascade was proven by the increased phosphorylation of eIF-2α, a translation complex component. This has as a consequence general attenuation of the protein synthesis, with exceptions being protein factors involved in UPR. It is tempting to speculate that this mechanism could be responsible for the lack of observed increase in p21 protein content. Another indirect evidence for the PERK pathway activation is observed cyclin D1 downregulation. Decreased cyclin D1 levels might be due to PERK/eIF-2α-mediated increase in cyclin D1 proteasomal degradation, independently of the translation efficacy (55). Activation of IRE1 arm of UPR by DHA was proven by the appearance of the spliced variant of XBP-1 transcription factor. This spliced variant cooperates with ATF4-ATF6 transcription factors, also activated by ER stress, to induce the expression of UPR responsive genes, including ER residing chaperon proteins like Bip. Indeed, increased levels of Bip were measured in DHA-treated hPASMC, indicative of UPR activation upon DHA treatment (Fig. 7).

Further support of activated ER stress response under DHA exposure in hPASMC was provided by a significantly increased expression of ER stress response genes Ero1-Lβ (Fig. 8). Protein folding in the ER requires an oxidizing environment for the generation of disulfide bonds (56). The redox peptide glutathione is important in regulating the rate of ER protein oxidation (57,58) and provides reducing equivalents for reductive/isomerization pathways (59). PDI is the major enzyme responsible for ER protein oxidation (60). PDI is maintained in the oxidized state by the oxidoreductase Ero1, which is essential for viability (61-63). In mammals, Ero1α is induced by hypoxia (64), whereas Ero1β is induced by the unfolded protein response (65). Expression of Ero1-Lα was increased in hPASMC exposed to 1% hypoxia (Fig. 8). Of note, 1% hypoxia alone did not cause an increase in ER stress marker genes in hPASMC (Fig. 8). The reason for this is not completely clear, however, taken together with the observed slower proliferation of hPASMC under hypoxia, it is tempting to speculate that in our experimental setup hPASMC enter a quiescent phase under hypoxia and therefore have decreased needs for protein synthesis. Under conditions of lower protein synthesis, it is to be expected that in the ER enter generally less proteins and thus the potential for overload with unfolded proteins is altogether lower, explaining the lack of upregulation of ER stress marker genes.

4.5. DHA-INDUCED CHANGES IN THE CELLULAR LIPID PROFILE

Since protein folding and posttranslational protein modifications are highly sensitive to alterations in the ER luminal environment, we examined first the impact of DHA on the cellular lipid composition. Beside a marked increase in DHA containing phospholipids, there was a striking decrease in PC and PE species containing mono- (18:1) and di- (18:2) unsaturated fatty acids (Fig. 9 A, B). DHA that has entered the cell and been activated to fatty acids acyl-CoA thioesters, can be incorporated in cellular phospholipids by two possible mechanisms. One is during de novo synthesis of cellular phosphatidylcholine and phosphatidylethanolamine species in the Kennedy pathway (66). However, DHA is

more likely incorporated into preexisting phospholipids that are continuously being modified by the cell during the course of the Lands cycle in which lysophospholipid species formed by the action of phospholipase A_2 are recycled back to phospholipid species by the action of lysophosphatidylcholine acyltransferase (67). In this respect, DHA might compete with 18:1, 18:2 and other fatty acids for lysophosphatidylcholine acyltransferase (LPCAT)-mediated incorporation into cellular phospholipids (68).

Interestingly, lipid profile seen in DHA-treated hPASMC is partly similar to that reported in HeLa cells, where stearoyl-CoA desaturase 1 (SCD1) knockdown decreased membrane phospholipid unsaturation, particularly 18:1 fatty acid, leading to UPR and apoptosis (69). Although SCD1 mRNA levels were not significantly altered by DHA in our study (not shown), the possibility remains that SCD1 activity is impaired by DHA leading to the observed lipid profile.

Increased incorporation of DHA into cellular phospholipids is indirectly supported by the observed increase in DHA-containing lysophospholipid species (Fig. 9C, D). Disturbed conformation and consequently dysfunction of ER-membrane associated chaperons, with concomitant accumulation of unfolded proteins, might therefore be an explanation for the observed induction of ER stress and UPR upon perturbations in the phospholipid composition. Finally, this experiment shows the efficient incorporation of DHA in cellular lipids.

4.6. DHA-INDUCED CHANGES IN CELLULAR REACTIVE OXYGEN SPECIES (ROS) PRODUCTION

HO-1 enzyme is an inducible isoform and serves as anti-oxidant defense and cellular protective factor. It is frequently up-regulated under stress conditions, including UPR (70), but also oxidative stress (71). Its high and early induction under DHA treatment (Fig. 10) led us to further investigate the potential role of oxidative stress in DHA-induced effects on UPR and proliferation in hPASMC. Of

note, in accordance with Ero1-Lα data, there was no increase in HO-1 expression under hypoxia exposure alone (Fig. 10).

In accordance with the HO-1 data, DHA induced a strong and rapid increase in ROS production measured by fluorescent ROS sensitive indicator dye (Fig. 11A). The observed DHA-induced ROS production was very rapid in onset suggesting that an acute cellular response to DHA is responsible for the initiation of UPR and the inhibition of hPASMC proliferation. Indeed, Tempol, a strong antioxidant and free radical scavenger, effectively blocked not only DHA-induced oxidative stress (Fig. 11B) but also rescued DHA-suppressed hPASMC proliferation (Fig. 11C and D) and ameliorated the ER stress response in DHA-treated hPASMC (Fig. 11E). These results clearly show increased ROS production as the main mechanism behind the DHA-induced UPR and subsequent anti-proliferative effect on hPASMC. Furthermore, the counteracting effect of Tempol establishes the increased production of free radicals as a driving force behind DHA-mediated effects. This correlates well with the observed increase in the expression of oxidoreductive enzymes such as Ero1-Lβ and HO-1, which mark the activation of cellular defense and repair mechanisms and attempt to cope with increased oxidative stress. However, HO-1 byproducts themselves have anti-proliferative effect (72), which could re-enforce direct DHA-mediated effects even further. The exact role of HO-1 in DHA-induced processes was investigated further in detail by Gabriel Stulnig as part of his diploma thesis work.

4.7. DHA-INDUCED CHANGES IN INTRACELLULAR CA^{2+} HOMEOSTASIS

It is known that changes in intracellular calcium homeostasis can lead to UPR (28) and are involved in the increased ROS production (73). Indeed, DHA induced a rapid increase in cytosolic calcium (Fig. 12B), a prerequisite for DHA-induced ROS formation (Fig. 11A). In line with the previously described mechanism of the DHA-induced increase in cytosolic calcium (74), both Ca^{2+} released from ER (Fig. 12A) and outside-in Ca^{2+} entry (Fig. 12C) contributed to the DHA-induced increase in

cytosolic Ca^{2+} levels, which triggered the ROS generation (Fig. 11A). Taken together, these results show the central role of intracellular calcium increase as the initial trigger of ROS production. Although not tested, it is tempting to speculate that the intracellular calcium chelator BAPTA-AM or extracellular EGTA would show similar DHA-antagonizing effect as free radical scavenger Tempol. It is thus possible to affect DHA-initiated processes in intracellular signaling cascade at different levels.

Importantly, prolonged exposure of cells to DHA (5 hours) did not alter the amount of ionomycin releasable Ca^{2+} (not shown), indicating that steady state ER Ca^{2+} levels were not altered upon prolonged exposure to DHA. Accordingly, depletion of ER Ca^{2+} seems not to be the trigger of ER stress and UPR in DHA treated cells. Rather, the DHA-induced Ca^{2+}-dependent oxidative stress.

Investigating downstream consequences of increased intracellular calcium, we tested the possibility that mitochondria are the site of increased ROS production. Indeed, experiments with RU360, an inhibitor of mitochondrial calcium uptake, and MitoSOX Red, mitochondrial specific redox sensor dye, showed that the calcium influx of Ca^{2+} into mitochondria was necessary for DHA-induced increase in ROS (Fig. 12D, E). Co-staining of DHA-treated hPASMC with the mitochondrial specific dye MitoTracker Green and MitoSOX Red and resulted in a strong overlap of the two signals, confirming high specificity of the MitoSOX Red signal as a measure for mitochondrial specific ROS production (Fig. 13).

Of note, the DHA-induced ROS increase was not completely abolished by RU3560 (Fig. 12D), indicating either an incomplete block of calcium influx or, more likely, additional intracellular sources of the DHA-induced ROS production. Since the DHA-induced mitochondrial ROS increase, measured by MitoSOX Red (Fig. 12E), was almost completely abolished with pre-treatment by RU360, but such effect was not seen in case of total cellular ROS, these results strongly point to other intracellular ROS production sites in addition to the mitochondria.

Although uncoupling of mitochondrial respiratory chain is frequently reported as a possible source of intracellular ROS (75), experiments with rotenone (mitochondrial respiratory chain complex I inhibitor) and TTFA (mitochondrial respiratory chain complex II inhibitor), did not show an effect on DHA-induced ROS production (Fig. 14). Additionally, general NADPH oxidase inhibitor DPI also did not have any effect (Fig. 14). Interestingly, cyclooxygenase (COX) inhibitor indomethacin increased both basal and DHA-induced ROS (Fig. 14). However, the exact role of COX enzymes in DHA effects was not investigated further.

4.8. DHA-INDUCED MITOCHONDRIAL DYSFUNCTION RESULTS IN APOPTOSIS OF HPASMC

It is well established that increased mitochondrial Ca^{2+} levels promote the opening of the permeability transition pores (PTP) in the mitochondrial inner membrane, leading to a decreased mitochondrial membrane potential ($\Delta\Psi_m$,), cytochrome c release and an inhibition of the respiratory chain at complex III, which is accompanied by an increased ROS production (76,77). These events eventually lead to the activation of the apoptotic cascade (78). Indeed, DHA induced apoptosis in hPASMC, evidenced by late apoptotic markers, cleaved caspase 3 (Fig. 15A) and DNA fragmentation by TUNEL assay (Fig. 15B). Considering the capacity of Ca^{2+} influx into mitochondria and concomitantly increased mitochondrial ROS to trigger apoptosis (79), it is conceivable that similar mechanism underlies DHA-induced apoptosis in this experimental system. We observed a Ca^{2+} dependent increase in mitochondrial ROS and an attenuating effect of Tempol on caspase-3 cleavage (Fig. 15C). Furthermore, DHA treatment decreased $\Delta\Psi_m$ in hPASMC (Fig. 15D), indicating the opening of the mitochondrial inner membrane PTP, an event associated with the release of proapoptotic molecules from mitochondria (80). Another evidence of mitochondrial dysfunction is the observed decrease in intracellular ATP content (Fig. 15E) and ATP to ADP ratio (Fig. 15F). It was shown that ATP-depletion by itself, independent of mitochondrial membrane depolarization, can lead to cell death (81).

Our results show that the DHA-induced increase of mitochondrial ROS is sensitive to RU360, together with a decreased $\Delta\Psi_m$ and ATP content, strongly argue for the role of DHA-induced cytosolic Ca^{2+} increase in mitochondrial dysfunction. However, mitochondria were not the only source of ROS in DHA treated cells, since overall cellular ROS were significantly decreased but not completely abolished with RU360 (Fig. 12D). This could help to explain the lack of an effect of RU360 on DHA-induced hPASMC proliferation inhibition (Fig. 16).

It has been shown that ROS may cause ER stress and that accumulation of misfolded proteins in ER lumen can initiate the ROS production (30,82,83). Considering a very rapid increase in DHA-induced ROS, preceding the increase in UPR markers, it is possible that the initial increase in ROS, generated outside of ER, affects the ER folding machinery leading to UPR and concomitant generation of ER-derived ROS.

Based on the capacity of Tempol to counteract the DHA-induced UPR, apoptosis and cell cycle arrest, the DHA-induced oxidative stress seems to be the initial event triggered by DHA. The failure of RU360 to counteract the DHA-mediated attenuation of hPASMC proliferation (Fig. 16), clearly demonstrates a rather weak relative contribution of mitochondrial ROS, suggesting contributions of various cellular ROS sources in triggering and mediating DHA effects in hPASMC. The exact intracellular localization and the relative quantitative and temporal contribution of various ROS sources in DHA-treated cells require further investigation. Whether and to what extent CHOP, a proapoptotic component of UPR (84,85) contributes to DHA-induced apoptosis remains to be determined. It is possible that the concomitant activation of the UPR leads to increased production of ER-originating ROS through the activity of Ero1 enzyme (30). Furthermore, same mechanism can at the same time have as a consequence a depletion of intracellular stores of glutathione (30).

In addition to the mitochondria and the ER, peroxisomes could also serve as a potential ROS source. Long chain fatty acids, such as DHA, can be oxidized in the peroxisomes with concomitant production of hydrogen peroxide (86). Furthermore, it was shown that DHA can lead to increased acyl-CoA oxidase activity (87), possibly increasing the peroxisomal ROS production.

4.9. DEVELOPMENT OF EXPERIMENTAL PULMONARY HYPERTENSION AND EFFECTS OF FISH OIL RICH DIET ON MICE

Although there are several different models of experimental pulmonary hypertension (16), they are all characterized by more or less pronounced proliferation of pulmonary vascular smooth muscle cells or, more generally, cells having a smooth muscle cell phenotype. We therefore speculated that compounds acting on vascular smooth muscle cells by either inhibiting their proliferation or inducing their apoptosis could have a clinically relevant therapeutic effect. Our in vitro experiments have shown that DHA and other members of omega-3 PUFA inhibit the proliferation and induce apoptosis of human pulmonary artery smooth muscle cells. Furthermore, we showed that the DHA anti-proliferative effect is present regardless of proliferation stimuli (hypoxia, PDGF-BB).

Based on these observations, we investigated the effect of omega-3 PUFA in an in vivo setting of experimental pulmonary hypertension.

We used hypoxia-induced pulmonary hypertension in mice as an experimental model. In this model, mice are exposed for several weeks to 10% hypoxia, which corresponds to oxygen levels at approximately 4000 meters above sea level (88). Hypoxic pulmonary vasoconstriction leads to an acute increase in pulmonary vascular resistance and increased pulmonary artery pressure. Prolonged exposure to hypoxia leads to pulmonary vascular and right ventricle remodeling.

In order to assess the effect of omega-3 PUFA, mice were fed with a special diet enriched with omega-3 fatty acids (fish oil diet). For comparison, two additional diet regiments were used: isocaloric control oil diet and chow mice diet. To assure the incorporation and saturation of the tissue lipids with omega-3 fatty acids, feeding was initiated two weeks before the planned start of hypoxia. Mass spectrometric analysis (Fig. 19) confirmed the robust accumulation of omega-3 fatty acids in lung lipids and the concomitant reduction in omega-6 fatty acids. These results are in line with observed DHA-induced changes in the lipid profile of hPASMC. To minimize fatty acid oxidation due to air exposure, food pellets were supplemented with lipophilic antioxidant vitamin E and food was changed daily.

Hypoxia exposed animals had a generally lower total body weight compared to the normoxic controls in all three tested feeding regiments (Fig. 17) and corn oil diet fed mice had a trend of higher body weight compared to fish oil and chow diet mice (Fig. 17).

Severe pulmonary hypertension and consequent right heart failure can lead to congestion in the venous system with detrimental effect on the liver (89). Blood congestion in the liver and thus indirectly right heart failure can be determined as increased liver weight. Although our results do not show increased liver weight in hypoxic animals, there is a trend of increased liver weight in fat-rich diets (both fish and corn oil) in both normoxic and hypoxic animals (Fig. 18). This can be best explained by metabolic consequences (fat accumulation due to increased nutritional supply) rather then pulmonary hypertension mediated hemodynamic changes.

Prolonged increase in the pulmonary vascular resistance, as a consequence of hypoxic vasoconstriction and vascular remodeling, leads to compensatory right ventricle hypertrophy (90). This is measured as increased weight ratio of right to left ventricle and septum (Fulton index). Therefore, any therapeutic amelioration in pulmonary vascular resistance could indirectly be detected as a decrease in Fulton index. As expected, hypoxia caused right ventricular hypertrophy (Fig. 20).

However, there was no significant difference between any of the tested diet regiments (Fig. 20). This result implies a lack of effect of omega-3 fatty acids rich diet on pulmonary vascular remodeling in this experimental setup.

Vessel wall thickening and a decrease in the vessel lumen size characterize pulmonary vascular remodeling in human pulmonary hypertension (7). However, measurement of percent vessel wall thickness in this mouse model of pulmonary hypertension (Fig. 21) proved to be time-consuming, unreliable and with low sensitivity (Fig. 22). Interestingly, trend for the most pronounced difference was observed on the level of the smallest measured vessels – ones in close proximity to the alveolar ducts (Fig. 22). This correlates well with observations from other groups that showed that the majority of pulmonary vascular remodeling in the hypoxia-induced mouse model happens on the level of the small parenchymal vessels with diameter less than 70 μm (15). Furthermore, this remodeling is best characterized as the appearance of smooth muscle cells around previously non-muscularized vessels (10). We conclude that the vessel wall thickness is inappropriate analysis method for quantifying pulmonary vascular remodeling in this animal model. Alternative analysis methods were not pursued further due to a lack of effect on the level of right ventricular hypertrophy (Fig. 20).

Gene expression analysis of oxidative and ER stress markers was performed in lung homogenates in order to clarify possible reasons behind the observed lack of effect of the fish oil diet.

Initial qRT-PCR analysis included the oxidative stress markers Ero1-L and HO-1 and the ER stress marker HSPA5. Although Ero1-Lβ did not show an increase in fish oil diet treated mice, HSPA5 showed a trend of increased expression in both normoxic and hypoxic fish oil diet treated mice (Fig. 23). Surprisingly, the gene expression of Ero1-Lα, a hypoxia responsive isoform, was only marginally increased in hypoxia-exposed mice (Fig. 23). On the other hand, a marker of global oxidative stress, HO-1 showed a tendency of higher expression levels under both fish oil diet and hypoxia exposure (Fig. 23). However, a more detailed

comparison of the gene expression levels of HO-1 and HSPA5 including all three different diet regiments revealed that the increased gene expression levels of HO-1 (Fig. 25) and HSPA5 (Fig. 26) are most pronounced in corn oil fed mice. Therefore, the most probable explanation for the tendential increase of these two markers in fish oil diet fed mice is the increased supply of fatty acids and subsequent metabolism, rather than specific effect of omega-3 fatty acids.

PUFA, including DHA, are known PPARγ ligands (91) and the activation of PPARγ pathway was shown to inhibit the proliferation of PASMC and reverse experimental pulmonary hypertension (92). Furthermore, DHA was shown to bind, activate and exert some of its effects also through other PPAR isoforms (93,94). Since PPARα is primarily expressed in the liver (95), we focused on delta and gamma isoforms.

Both PPARδ and PPARγ are expressed in mouse lungs (Fig. 23). Of note, hypoxia seems to increase the expression level of PPARδ (Fig. 23). A possible activation of PPAR pathway was indirectly assessed by investigating gene expression levels of all three PPAR isoform marker genes (96-99). However, none of tested genes showed an indication of PPAR signaling pathway activation with fish oil diet (Fig. 24).

It could be speculated that the lack of fish oil diet effect in mice could be due to pharmacokinetic differences when compared to in vitro situation. Although n-3 PUFA accumulates in the lung lipid fraction, the way this is achieved is quite different in comparison when cells are exposed to DHA. In the case of animals, n-3 PUFA are delivered to PASMC indirectly by circulation. After ingestion, majority of DHA and other n-3 PUFA are packaged into triglycerides and phospholipids of VLDL and LDL particles (87). Furthermore, remaining part of free fatty acids is also transported in the blood bound to plasma proteins, in particular albumin (87). This leaves only a small fraction of free DHA to act acutely on cells. Taken together, these mechanisms lead to buffered supply of DHA and other n-3 PUFA to the PASMC. This allows prolonged supply of lower effective concentration of n-

3 PUFA, which is sufficient for enrichment of lung lipids in n-3 PUFA, but not sufficient for initiating molecular events seen in vitro. On the other hand, direct acute application of a single high DHA concentration to cells likely exceeds the buffering capacity of albumin present in the medium. Furthermore, lipoprotein particles present in the cell medium do not in this case, serve as an additional buffer and extended-release reservoir of DHA.

Finally, the fish oil rich diet contains as a standard addition potent lipophilic antioxidant – vitamin E (Table 4). Taking in consideration the antagonizing effect of free radical scavenger Tempol, it is possible that the concomitant presence of antioxidant compound in could additionally blunt the effectiveness of n-3 PUFA rich diet.

5. CONCLUSIONS

Based on the results of the performed comprehensive analysis of molecular events in DHA treated primary hPASMC, we conclude that Ca^{2+}-dependent induction of oxidative stress is the central and initial event responsible for the induction of UPR, cell cycle arrest and apoptosis in DHA treated hPASMC. The major, but not exclusive, source of this oxidative stress was mitochondria. Furthermore, DHA showed the most potent effect on inhibition of hPASMC proliferation of all tested n-3 PUFA, including EPA and alpha-linolenic acid. The results show a simultaneous activation and an overlap of several different mechanisms (UPR, oxidative stress, disturbances in calcium homeostasis and lipid composition) that are present at the same time and possibly potentiate each other.

The fact that the DHA-mediated induction of oxidative stress, UPR and apoptosis might be beneficial in SMC undergoing remodeling (pulmonary hypertension or stent restenosis), but detrimental in SMC constituting a cap of a stable atherosclerotic plaque (100), implicates that a systemic application of DHA may simultaneously be both beneficial and harmful. This is of importance, as these pathologic states may co-exist in a patient.

Using an experimental animal model of pulmonary hypertension, we could not observe an improvement in right ventricular hypertrophy in mice fed with omega-3 PUFA rich diet (fish oil). This is despite the observed effect on lung lipid composition in which lung lipids were significantly enriched in omega-3 PUFAs. Furthermore, there was no significant or specific activation of UPR marker genes in mice fed with fish oil diet. Finally, there was no indication of PPAR pathway activation in fish oil diet fed mice. Pharmacokinetic reasons (packaging of dietary n-3 PUFA into lipoprotein particles and binding to plasma proteins) might leads to a more gradual delivery of bioactive free n-3 PUFA to lung vascular smooth muscle cells when compared to acute, high dosing of DHA in in vitro condition.

6. BIBLIOGRAPHY

(1) Humbert M, Morrell NW, Archer SL, Stenmark KR, MacLean MR, Lang IM, et al. Cellular and molecular pathobiology of pulmonary arterial hypertension. J Am Coll Cardiol 2004 Jun 16;43(12 Suppl S):13S-24S.

(2) Landzberg BR, Frishman WH, Lerrick K. Pathophysiology and pharmacological approaches for prevention of coronary artery restenosis following coronary artery balloon angioplasty and related procedures. Prog Cardiovasc Dis 1997 Jan-Feb;39(4):361-398.

(3) Archer SL, Weir EK, Wilkins MR. Basic science of pulmonary arterial hypertension for clinicians: new concepts and experimental therapies. Circulation 2010 May 11;121(18):2045-2066.

(4) Galie N, Torbicki A, Barst R, Dartevelle P, Haworth S, Higenbottam T, et al. Guidelines on diagnosis and treatment of pulmonary arterial hypertension. The Task Force on Diagnosis and Treatment of Pulmonary Arterial Hypertension of the European Society of Cardiology. Eur Heart J 2004 Dec;25(24):2243-2278.

(5) Humbert M, Morrell NW, Archer SL, Stenmark KR, MacLean MR, Lang IM, et al. Cellular and molecular pathobiology of pulmonary arterial hypertension. J Am Coll Cardiol 2004 Jun 16;43(12 Suppl S):13S-24S.

(6) Budhiraja R, Tuder RM, Hassoun PM. Endothelial dysfunction in pulmonary hypertension. Circulation 2004 Jan 20;109(2):159-165.

(7) Stacher E, Graham BB, Hunt JM, Gandjeva A, Groshong SD, McLaughlin VV, et al. Modern age pathology of pulmonary arterial hypertension. Am J Respir Crit Care Med 2012 Aug 1;186(3):261-272.

(8) WOOD P. Pulmonary hypertension with special reference to the vasoconstrictive factor. Br Heart J 1958 Oct;20(4):557-570.
(9) Yuan JX, Aldinger AM, Juhaszova M, Wang J, Conte JV,Jr, Gaine SP, et al. Dysfunctional voltage-gated K+ channels in pulmonary artery smooth muscle cells of patients with primary pulmonary hypertension. Circulation 1998 Oct 6;98(14):1400-1406.

(10) Stenmark KR, Meyrick B, Galie N, Mooi WJ, McMurtry IF. Animal models of pulmonary arterial hypertension: the hope for etiological discovery and pharmacological cure. Am J Physiol Lung Cell Mol Physiol 2009 Dec;297(6):L1013-32.

(11) Cowan KN, Heilbut A, Humpl T, Lam C, Ito S, Rabinovitch M. Complete reversal of fatal pulmonary hypertension in rats by a serine elastase inhibitor. Nat Med 2000 Jun;6(6):698-702.

(12) Pietra GG, Capron F, Stewart S, Leone O, Humbert M, Robbins IM, et al. Pathologic assessment of vasculopathies in pulmonary hypertension. J Am Coll Cardiol 2004 Jun 16;43(12 Suppl S):25S-32S.

(13) Dorfmuller P, Perros F, Balabanian K, Humbert M. Inflammation in pulmonary arterial hypertension. Eur Respir J 2003 Aug;22(2):358-363.

(14) Friedman R, Mears JG, Barst RJ. Continuous infusion of prostacyclin normalizes plasma markers of endothelial cell injury and platelet aggregation in primary pulmonary hypertension. Circulation 1997 Nov 4;96(9):2782-2784.

(15) Schermuly RT, Dony E, Ghofrani HA, Pullamsetti S, Savai R, Roth M, et al. Reversal of experimental pulmonary hypertension by PDGF inhibition. J Clin Invest 2005 Oct;115(10):2811-2821.

(16) Ryan J, Bloch K, Archer SL. Rodent models of pulmonary hypertension: harmonisation with the world health organisation's categorisation of human PH. Int J Clin Pract Suppl 2011 Aug;(172):15-34. doi(172):15-34.

(17) Russo GL. Dietary n-6 and n-3 polyunsaturated fatty acids: from biochemistry to clinical implications in cardiovascular prevention. Biochem Pharmacol 2009 Mar 15;77(6):937-946.

(18) Dietary supplementation with n-3 polyunsaturated fatty acids and vitamin E after myocardial infarction: results of the GISSI-Prevenzione trial. Gruppo Italiano per lo Studio della Sopravvivenza nell'Infarto miocardico. Lancet 1999 Aug 7;354(9177):447-455.

(19) Gissi-HF Investigators, Tavazzi L, Maggioni AP, Marchioli R, Barlera S, Franzosi MG, et al. Effect of n-3 polyunsaturated fatty acids in patients with chronic heart failure (the GISSI-HF trial): a randomised, double-blind, placebo-controlled trial. Lancet 2008 Oct 4;372(9645):1223-1230.

(20) Pakala R, Pakala R, Sheng WL, Benedict CR. Vascular smooth muscle cells preloaded with eicosapentaenoic acid and docosahexaenoic acid fail to respond to serotonin stimulation. Atherosclerosis 2000 Nov;153(1):47-57.

(21) Terano T, Tanaka T, Tamura Y, Kitagawa M, Higashi H, Saito Y, et al. Eicosapentaenoic acid and docosahexaenoic acid inhibit vascular smooth muscle cell proliferation by inhibiting phosphorylation of Cdk2-cyclinE complex. Biochem Biophys Res Commun 1999 Jan 19;254(2):502-506.

(22) Terano T, Shiina T, Tamura Y. Eicosapentaenoic acid suppressed the proliferation of vascular smooth muscle cells through modulation of various steps of growth signals. Lipids 1996 Mar;31 Suppl:S301-4.

(23) Jakobsen CH, Storvold GL, Bremseth H, Follestad T, Sand K, Mack M, et al. DHA induces ER stress and growth arrest in human colon cancer cells: associations with cholesterol and calcium homeostasis. J Lipid Res 2008 Oct;49(10):2089-2100.

(24) Leonardi F, Attorri L, Benedetto RD, Biase AD, Sanchez M, Tregno FP, et al. Docosahexaenoic acid supplementation induces dose and time dependent oxidative changes in C6 glioma cells. Free Radic Res 2007 Jul;41(7):748-756.
(25) Prasad A, Bloom MS, Carpenter DO. Role of calcium and ROS in cell death induced by polyunsaturated fatty acids in murine thymocytes. J Cell Physiol 2010 Nov;225(3):829-836.

(26) Shiina T, Terano T, Saito J, Tamura Y, Yoshida S. Eicosapentaenoic acid and docosahexaenoic acid suppress the proliferation of vascular smooth muscle cells. Atherosclerosis 1993 Dec;104(1-2):95-103.

(27) Diep QN, Touyz RM, Schiffrin EL. Docosahexaenoic acid, a peroxisome proliferator-activated receptor-alpha ligand, induces apoptosis in vascular smooth muscle cells by stimulation of p38 mitogen-activated protein kinase. Hypertension 2000 Nov;36(5):851-855.

(28) Schroder M, Kaufman RJ. Divergent roles of IRE1alpha and PERK in the unfolded protein response. Curr Mol Med 2006 Feb;6(1):5-36.

(29) Kim I, Xu W, Reed JC. Cell death and endoplasmic reticulum stress: disease relevance and therapeutic opportunities. Nat Rev Drug Discov 2008 Dec;7(12):1013-1030.

(30) Santos CX, Tanaka LY, Wosniak J, Laurindo FR. Mechanisms and implications of reactive oxygen species generation during the unfolded protein response: roles of endoplasmic reticulum oxidoreductases, mitochondrial electron

transport, and NADPH oxidase. Antioxid Redox Signal 2009 Oct;11(10):2409-2427.

(31) Olschewski A, Li Y, Tang B, Hanze J, Eul B, Bohle RM, et al. Impact of TASK-1 in human pulmonary artery smooth muscle cells. Circ Res 2006 Apr 28;98(8):1072-1080.

(32) Hallstrom S, Gasser H, Neumayer C, Fugl A, Nanobashvili J, Jakubowski A, et al. S-nitroso human serum albumin treatment reduces ischemia/reperfusion injury in skeletal muscle via nitric oxide release. Circulation 2002 Jun 25;105(25):3032-3038.

(33) Furst W, Hallstrom S. Simultaneous determination of myocardial nucleotides, nucleosides, purine bases and creatine phosphate by ion-pair high-performance liquid chromatography. J Chromatogr 1992 Jul 1;578(1):39-44.

(34) Bligh EG, Dyer WJ. A rapid method of total lipid extraction and purification. Can J Biochem Physiol 1959 Aug;37(8):911-917.

(35) Hartler J, Trotzmuller M, Chitraju C, Spener F, Kofeler HC, Thallinger GG. Lipid Data Analyzer: unattended identification and quantitation of lipids in LC-MS data. Bioinformatics 2011 Feb 15;27(4):572-577.

(36) Riederer M, Ojala PJ, Hrzenjak A, Graier WF, Malli R, Tritscher M, et al. Acyl chain-dependent effect of lysophosphatidylcholine on endothelial prostacyclin production. J Lipid Res 2010 Oct;51(10):2957-2966.

(37) Graier WF, Simecek S, Sturek M. Cytochrome P450 mono-oxygenase-regulated signalling of Ca2+ entry in human and bovine endothelial cells. J Physiol 1995 Jan 15;482 (Pt 2)(Pt 2):259-274.

(38) Bousserouel S, Raymondjean M, Brouillet A, Bereziat G, Andreani M. Modulation of cyclin D1 and early growth response factor-1 gene expression in interleukin-1beta-treated rat smooth muscle cells by n-6 and n-3 polyunsaturated fatty acids. Eur J Biochem 2004 Nov;271(22):4462-4473.

(39) Elvevoll EO, Barstad H, Breimo ES, Brox J, Eilertsen KE, Lund T, et al. Enhanced incorporation of n-3 fatty acids from fish compared with fish oils. Lipids 2006 Dec;41(12):1109-1114.

(40) Rusca A, Di Stefano AF, Doig MV, Scarsi C, Perucca E. Relative bioavailability and pharmacokinetics of two oral formulations of docosahexaenoic acid/eicosapentaenoic acid after multiple-dose administration in healthy volunteers. Eur J Clin Pharmacol 2009 May;65(5):503-510.

(41) Cao J, Schwichtenberg KA, Hanson NQ, Tsai MY. Incorporation and clearance of omega-3 fatty acids in erythrocyte membranes and plasma phospholipids. Clin Chem 2006 Dec;52(12):2265-2272.

(42) Harper CR, Edwards MJ, DeFilippis AP, Jacobson TA. Flaxseed oil increases the plasma concentrations of cardioprotective (n-3) fatty acids in humans. J Nutr 2006 Jan;136(1):83-87.

(43) Clore JN, Allred J, White D, Li J, Stillman J. The role of plasma fatty acid composition in endogenous glucose production in patients with type 2 diabetes mellitus. Metabolism 2002 Nov;51(11):1471-1477.

(44) Raghavan A, Zhou G, Zhou Q, Ibe JC, Ramchandran R, Yang Q, et al. Hypoxia-induced pulmonary arterial smooth muscle cell proliferation is controlled by forkhead box M1. Am J Respir Cell Mol Biol 2012 Apr;46(4):431-436.

(45) Yang X, Sheares KK, Davie N, Upton PD, Taylor GW, Horsley J, et al. Hypoxic induction of cox-2 regulates proliferation of human pulmonary artery smooth muscle cells. Am J Respir Cell Mol Biol 2002 Dec;27(6):688-696.

(46) Howard LS, Crosby A, Vaughan P, Sobolewski A, Southwood M, Foster ML, et al. Distinct responses to hypoxia in subpopulations of distal pulmonary artery cells contribute to pulmonary vascular remodeling in emphysema. Pulm Circ 2012 Apr-Jun;2(2):241-249.

(47) De Caterina R, Bernini W, Carluccio MA, Liao JK, Libby P. Structural requirements for inhibition of cytokine-induced endothelial activation by unsaturated fatty acids. J Lipid Res 1998 May;39(5):1062-1070.

(48) Siemeister G, Lucking U, Wengner AM, Lienau P, Steinke W, Schatz C, et al. BAY 1000394, a novel cyclin-dependent kinase inhibitor, with potent antitumor activity in mono- and in combination treatment upon oral application. Mol Cancer Ther 2012 Oct;11(10):2265-2273.

(49) Sabir M, Baig RM, Mahjabeen I, Kayani MA. Significance of cyclin D1 polymorphisms in patients with head and neck cancer. Int J Biol Markers 2012 Nov 5:0.

(50) Wakino S, Kintscher U, Kim S, Yin F, Hsueh WA, Law RE. Peroxisome proliferator-activated receptor gamma ligands inhibit retinoblastoma phosphorylation and G1--> S transition in vascular smooth muscle cells. J Biol Chem 2000 Jul 21;275(29):22435-22441.

(51) Albino AP, Juan G, Traganos F, Reinhart L, Connolly J, Rose DP, et al. Cell cycle arrest and apoptosis of melanoma cells by docosahexaenoic acid: association with decreased pRb phosphorylation. Cancer Res 2000 Aug 1;60(15):4139-4145.

(52) Liu BQ, Gao YY, Niu XF, Xie JS, Meng X, Guan Y, et al. Implication of unfolded protein response in resveratrol-induced inhibition of K562 cell proliferation. Biochem Biophys Res Commun 2010 Jan 1;391(1):778-782.

(53) Jakobsen CH, Storvold GL, Bremseth H, Follestad T, Sand K, Mack M, et al. DHA induces ER stress and growth arrest in human colon cancer cells: associations with cholesterol and calcium homeostasis. J Lipid Res 2008 Oct;49(10):2089-2100.

(54) Caviglia JM, Gayet C, Ota T, Hernandez-Ono A, Conlon DM, Jiang H, et al. Different fatty acids inhibit apolipoprotein B100 secretion by different pathways: Unique roles for endoplasmic reticulum stress, ceramide, and autophagy. J Lipid Res 2011 Jun 30.

(55) Raven JF, Baltzis D, Wang S, Mounir Z, Papadakis AI, Gao HQ, et al. PKR and PKR-like endoplasmic reticulum kinase induce the proteasome-dependent degradation of cyclin D1 via a mechanism requiring eukaryotic initiation factor 2alpha phosphorylation. J Biol Chem 2008 Feb 8;283(6):3097-3108.

(56) Hwang C, Sinskey AJ, Lodish HF. Oxidized redox state of glutathione in the endoplasmic reticulum. Science 1992 Sep 11;257(5076):1496-1502.

(57) Molteni SN, Fassio A, Ciriolo MR, Filomeni G, Pasqualetto E, Fagioli C, et al. Glutathione limits Ero1-dependent oxidation in the endoplasmic reticulum. J Biol Chem 2004 Jul 30;279(31):32667-32673.

(58) Chakravarthi S, Bulleid NJ. Glutathione is required to regulate the formation of native disulfide bonds within proteins entering the secretory pathway. J Biol Chem 2004 Sep 17;279(38):39872-39879.

(59) Jessop CE, Bulleid NJ. Glutathione directly reduces an oxidoreductase in the endoplasmic reticulum of mammalian cells. J Biol Chem 2004 Dec 31;279(53):55341-55347.

(60) Wilkinson B, Gilbert HF. Protein disulfide isomerase. Biochim Biophys Acta 2004 Jun 1;1699(1-2):35-44.

(61) Pollard MG, Travers KJ, Weissman JS. Ero1p: a novel and ubiquitous protein with an essential role in oxidative protein folding in the endoplasmic reticulum. Mol Cell 1998 Jan;1(2):171-182.

(62) Frand AR, Kaiser CA. The ERO1 gene of yeast is required for oxidation of protein dithiols in the endoplasmic reticulum. Mol Cell 1998 Jan;1(2):161-170.

(63) Tu BP, Ho-Schleyer SC, Travers KJ, Weissman JS. Biochemical basis of oxidative protein folding in the endoplasmic reticulum. Science 2000 Nov 24;290(5496):1571-1574.

(64) Gess B, Hofbauer KH, Wenger RH, Lohaus C, Meyer HE, Kurtz A. The cellular oxygen tension regulates expression of the endoplasmic oxidoreductase ERO1-Lalpha. Eur J Biochem 2003 May;270(10):2228-2235.

(65) Pagani M, Fabbri M, Benedetti C, Fassio A, Pilati S, Bulleid NJ, et al. Endoplasmic reticulum oxidoreductin 1-lbeta (ERO1-Lbeta), a human gene induced in the course of the unfolded protein response. J Biol Chem 2000 Aug 4;275(31):23685-23692.

(66) Gibellini F, Smith TK. The Kennedy pathway--De novo synthesis of phosphatidylethanolamine and phosphatidylcholine. IUBMB Life 2010 Jun;62(6):414-428.

(67) Eto M, Shindou H, Koeberle A, Harayama T, Yanagida K, Shimizu T. Lysophosphatidylcholine Acyltransferase 3 Is the Key Enzyme for Incorporating Arachidonic Acid into Glycerophospholipids during Adipocyte Differentiation. Int J Mol Sci 2012 Dec 3;13(12):16267-16280.

(68) Perez-Chacon G, Astudillo AM, Balgoma D, Balboa MA, Balsinde J. Control of free arachidonic acid levels by phospholipases A2 and lysophospholipid acyltransferases. Biochim Biophys Acta 2009 Dec;1791(12):1103-1113.

(69) Ariyama H, Kono N, Matsuda S, Inoue T, Arai H. Decrease in membrane phospholipid unsaturation induces unfolded protein response. J Biol Chem 2010 Jul 16;285(29):22027-22035.

(70) Zheng M, Kim SK, Joe Y, Back SH, Cho HR, Kim HP, et al. Sensing endoplasmic reticulum stress by protein kinase RNA-like endoplasmic reticulum kinase promotes adaptive mitochondrial DNA biogenesis and cell survival via heme oxygenase-1/carbon monoxide activity. FASEB J 2012 Jun;26(6):2558-2568.

(71) Kusunoki C, Yang L, Yoshizaki T, Nakagawa F, Ishikado A, Kondo M, et al. Omega-3 polyunsaturated fatty acid has an anti-oxidant effect via the Nrf-2/HO-1 pathway in 3T3-L1 adipocytes. Biochem Biophys Res Commun 2012 Nov 3.

(72) Vitali SH, Mitsialis SA, Liang OD, Liu X, Fernandez-Gonzalez A, Christou H, et al. Divergent cardiopulmonary actions of heme oxygenase enzymatic products in chronic hypoxia. PLoS One 2009 Jun 19;4(6):e5978.

(73) Espino J, Bejarano I, Paredes SD, Gonzalez D, Barriga C, Reiter RJ, et al. Melatonin counteracts alterations in oxidative metabolism and cell viability induced by intracellular calcium overload in human leucocytes: changes with age. Basic Clin Pharmacol Toxicol 2010 Jul;107(1):590-597.

(74) Aires V, Hichami A, Filomenko R, Ple A, Rebe C, Bettaieb A, et al. Docosahexaenoic acid induces increases in [Ca2+]i via inositol 1,4,5-triphosphate production and activates protein kinase C gamma and -delta via phosphatidylserine binding site: implication in apoptosis in U937 cells. Mol Pharmacol 2007 Dec;72(6):1545-1556.

(75) Tonin AM, Amaral AU, Busanello EN, Grings M, Castilho RF, Wajner M. Long-chain 3-hydroxy fatty acids accumulating in long-chain 3-hydroxyacyl-CoA dehydrogenase and mitochondrial trifunctional protein deficiencies uncouple oxidative phosphorylation in heart mitochondria. J Bioenerg Biomembr 2012 Oct 13.

(76) Scorrano L, Penzo D, Petronilli V, Pagano F, Bernardi P. Arachidonic acid causes cell death through the mitochondrial permeability transition. Implications for tumor necrosis factor-alpha aopototic signaling. J Biol Chem 2001 Apr 13;276(15):12035-12040.

(77) Starkov AA, Chinopoulos C, Fiskum G. Mitochondrial calcium and oxidative stress as mediators of ischemic brain injury. Cell Calcium 2004 Sep-Oct;36(3-4):257-264.

(78) Kuznetsov AV, Margreiter R, Amberger A, Saks V, Grimm M. Changes in mitochondrial redox state, membrane potential and calcium precede mitochondrial dysfunction in doxorubicin-induced cell death. Biochim Biophys Acta 2011 Jun;1813(6):1144-1152.

(79) Chinopoulos C, Adam-Vizi V. Calcium, mitochondria and oxidative stress in neuronal pathology. Novel aspects of an enduring theme. FEBS J 2006 Feb;273(3):433-450.

(80) Szabadkai G, Rizzuto R. Participation of endoplasmic reticulum and mitochondrial calcium handling in apoptosis: more than just neighborhood? FEBS Lett 2004 Jun 1;567(1):111-115.

(81) Nieminen AL, Saylor AK, Herman B, Lemasters JJ. ATP depletion rather than mitochondrial depolarization mediates hepatocyte killing after metabolic inhibition. Am J Physiol 1994 Jul;267(1 Pt 1):C67-74.

(82) Malhotra JD, Kaufman RJ. Endoplasmic reticulum stress and oxidative stress: a vicious cycle or a double-edged sword? Antioxid Redox Signal 2007 Dec;9(12):2277-2293.

(83) Malhotra JD, Miao H, Zhang K, Wolfson A, Pennathur S, Pipe SW, et al. Antioxidants reduce endoplasmic reticulum stress and improve protein secretion. Proc Natl Acad Sci U S A 2008 Nov 25;105(47):18525-18530.

(84) Marciniak SJ, Yun CY, Oyadomari S, Novoa I, Zhang Y, Jungreis R, et al. CHOP induces death by promoting protein synthesis and oxidation in the stressed endoplasmic reticulum. Genes Dev 2004 Dec 15;18(24):3066-3077.

(85) McCullough KD, Martindale JL, Klotz LO, Aw TY, Holbrook NJ. Gadd153 sensitizes cells to endoplasmic reticulum stress by down-regulating Bcl2 and perturbing the cellular redox state. Mol Cell Biol 2001 Feb;21(4):1249-1259.

(86) Ferdinandusse S, Denis S, Mooijer PA, Zhang Z, Reddy JK, Spector AA, et al. Identification of the peroxisomal beta-oxidation enzymes involved in the biosynthesis of docosahexaenoic acid. J Lipid Res 2001 Dec;42(12):1987-1995.

(87) Kim HK, Choi H. Stimulation of acyl-CoA oxidase by alpha-linolenic acid-rich perilla oil lowers plasma triacylglycerol level in rats. Life Sci 2005 Aug 5;77(12):1293-1306.

(88) Gallagher SA, Hackett PH. High-altitude illness. Emerg Med Clin North Am 2004 May;22(2):329-55, viii.

(89) Nikolaou M, Parissis J, Yilmaz MB, Seronde MF, Kivikko M, Laribi S, et al. Liver function abnormalities, clinical profile, and outcome in acute decompensated heart failure. Eur Heart J 2012 Oct 22.

(90) Bogaard HJ, Abe K, Vonk Noordegraaf A, Voelkel NF. The right ventricle under pressure: cellular and molecular mechanisms of right-heart failure in pulmonary hypertension. Chest 2009 Mar;135(3):794-804.

(91) Draper E, Reynolds CM, Canavan M, Mills KH, Loscher CE, Roche HM. Omega-3 fatty acids attenuate dendritic cell function via NF-kappaB independent of PPARgamma. J Nutr Biochem 2011 Aug;22(8):784-790.

(92) Hansmann G, de Jesus Perez VA, Alastalo TP, Alvira CM, Guignabert C, Bekker JM, et al. An antiproliferative BMP-2/PPARgamma/apoE axis in human and murine SMCs and its role in pulmonary hypertension. J Clin Invest 2008 May;118(5):1846-1857.

(93) Georgiadi A, Lichtenstein L, Degenhardt T, Boekschoten MV, van Bilsen M, Desvergne B, et al. Induction of cardiac Angptl4 by dietary fatty acids is mediated by peroxisome proliferator-activated receptor beta/delta and protects against fatty acid-induced oxidative stress. Circ Res 2010 Jun 11;106(11):1712-1721.

(94) Zuniga J, Cancino M, Medina F, Varela P, Vargas R, Tapia G, et al. N-3 PUFA supplementation triggers PPAR-alpha activation and PPAR-alpha/NF-kappaB interaction: anti-inflammatory implications in liver ischemia-reperfusion injury. PLoS One 2011;6(12):e28502.

(95) Oyekan A. PPARs and their effects on the cardiovascular system. Clin Exp Hypertens 2011;33(5):287-293.

(96) Borland MG, Khozoie C, Albrecht PP, Zhu B, Lee C, Lahoti TS, et al. Stable over-expression of PPARbeta/delta and PPARgamma to examine receptor signaling in human HaCaT keratinocytes. Cell Signal 2011 Dec;23(12):2039-2050.

(97) Pendse AA, Johnson LA, Kim HS, McNair M, Nipp CT, Wilhelm C, et al. Pro- and antiatherogenic effects of a dominant-negative P465L mutation of peroxisome proliferator-activated receptor-gamma in apolipoprotein E-Null mice. Arterioscler Thromb Vasc Biol 2012 Jun;32(6):1436-1444.

(98) Sanderson LM, Degenhardt T, Koppen A, Kalkhoven E, Desvergne B, Muller M, et al. Peroxisome proliferator-activated receptor beta/delta (PPARbeta/delta) but not PPARalpha serves as a plasma free fatty acid sensor in liver. Mol Cell Biol 2009 Dec;29(23):6257-6267.

(99) Kurokawa T, Shimomura Y, Bajotto G, Kotake K, Arikawa T, Ito N, et al. Peroxisome proliferator-activated receptor alpha (PPARalpha) mRNA expression in human hepatocellular carcinoma tissue and non-cancerous liver tissue. World J Surg Oncol 2011 Dec 15;9:167-7819-9-167.

(100) Tabas I. The role of endoplasmic reticulum stress in the progression of atherosclerosis. Circ Res 2010 Oct 1;107(7):839-850.

7. APPENDIX

Following publication resulted from this dissertation:

Crnkovic S, Riederer M, Lechleitner M, Hallström S, Malli R, Graier WF, Lindenmann J, Popper H, Olschewski H, Olschewski A, Frank S. Docosahexaenoic acid-induced unfolded protein response, cell cycle arrest, and apoptosis in vascular smooth muscle cells are triggered by Ca^{2+}-dependent induction of oxidative stress. Free Radic Biol Med. 2012 May 1;52(9):1786-95.